**PAPER**

# Temporal and spatial variability of cross-fault groundwater-level differences: the impact of fault-induced permeability reduction, precipitation and evapotranspiration

Rimbaud E. Lapperre[1] · Victor F. Bense[2] · Cornelis Kasse[1] · Ronald T. van Balen[1,3]

## Abstract

Faults in the Roer Valley Rift System (Netherlands, Belgium, and Germany) act as barriers to lateral groundwater flow in unconsolidated sedimentary aquifers. This causes a cross-fault groundwater-level step of up to several metres. Using a dataset obtained through 5 years of high-frequency monitoring, the effect of fault-zone permeability, precipitation and evapotranspiration on cross-fault groundwater-level steps is studied at two sites situated across the Peel Boundary Fault. Hydraulic conductivity values at the fault are 1–3 orders of magnitude lower than that of similar lithologies away from the fault, indicating that fault displacement has a significant impact on groundwater flow. The influence of precipitation and evapotranspiration on fault-zone hydrology is inferred from water-table fluctuations over short distances across the fault. On the foot wall, the water table is nearer to the surface and displays a shorter level range with a spiky temporal variability. On the hanging wall, a deeper water table is sloping away from the fault and shows a wider level range with a smoother temporal variability. The observed groundwater level fluctuations are attributed mainly to precipitation and evapotranspiration dynamics. At a larger spatial scale, the 5-year-average cross-fault groundwater-level steps at the two sites are 1.59 and 1.39 m. At a smaller scale, the cross-fault groundwater-level step is much less because of the rising water table towards the fault on the hanging wall. At the smallest scale, just across the fault zone, the groundwater level step is around 0.2 m, indicating that the fault is semi-impermeable.

## Introduction

The Roer Valley Rift System (RVRS) is an active rift system in the southeastern part of the Netherlands and adjoining areas in Belgium and Germany, and forms the northwestern continuation of the Lower Rhine Embayment. The RVRS (Fig. 1) consists of a series of horsts and grabens which are bounded by northwest–southeast-oriented fault zones (Van Balen et al.

2005, 2019), the most prominent of which are the Feldbiss Fault zone (FFZ), Peel Boundary Fault zone (PBFZ) and Tegelen Fault zone (TFZ; Fig. 2a). These and other fault zones in the RVRS act as (near) vertical barriers for lateral groundwater flow, causing pronounced steps in water-table elevation (Bense 2004; Bense and Van Balen 2004; Bense et al. 2013; Deckers et al. 2018; Lapperre et al. 2019). The sealing of these fault zones results from juxtaposition of stratigraphic units with contrasting permeability and the reduction in permeability resulting from clay smear in the fault core, rotation of elongated sediment grains, tectonic mixing of sediments with different grain-size and the precipitation of minerals such as iron (hydro)oxides in pore space (Bense et al. 2003b).

A review by Lapperre et al. (2019) reveals a wide range in phreatic cross-fault groundwater-level steps varying over almost 2 orders of magnitude, from 0.5 to 12.7 m. However, their review results are mainly based on groundwater level measurements at single moments in time during different years, and often without accurate specification of the exact

✉ Rimbaud E. Lapperre
r.e.lapperre@vu.nl

[1] Department of Earth Sciences, VU University Amsterdam, De Boelelaan 1085, 1081 HV Amsterdam, The Netherlands

[2] Wageningen University and Research, Droevendaalsesteeg 3, 6708 PB Wageningen, The Netherlands

[3] TNO - Geological Survey of the Netherlands, Princetonlaan 6, 3584 CB Utrecht, The Netherlands

🕱 Springer

location or detailed knowledge of the precision and accuracy of the groundwater level measurements. Therefore, it is unclear whether and to what extent seasonal variations in precipitation, evapotranspiration and site-specific circumstances such as land drainage and groundwater abstractions contribute to the large range of observed phreatic cross-fault groundwater levels in the RVRS (Lapperre et al. 2019).

In this study, time series of water-table-elevation measurements are used from two sites which have been monitored continuously for 5 years to study the influence of fault-zone hydrogeology, precipitation and evapotranspiration on temporal and spatial variation in cross-fault groundwater-level steps. The Bakel monitoring location (Bakel site) is located on a fault of the PBFZ (Fig. 1) where a trench was excavated in 2014 to study the lithostratigraphy, the fault displacement rates and the paleoseismicity (Van Balen et al. 2019), and where a groundwater level step is observed. After the trench was studied, the excavation was restored according to the preexisting sequence and the excavated fault rebuilt with low-permeability (sandy) loam. A cross-fault array of eight phreatic piezometers was installed and permanently monitored (2015–2020). The Geneneind monitoring location (Geneneind site) is situated northwest from the Bakel site, across the same fault (Fig. 2b). High-frequency monitoring data on groundwater levels were collected during the same time span. This paper presents the outcome of multiyear (2015–2020) and high-frequency phreatic groundwater-level measurements of the cross-fault piezometer arrays at the Bakel and Geneneind sites and provides an analysis of the influence of fault-zone permeability, precipitation and evapotranspiration on the recorded level variations. The hydrogeological findings from both sites across the Peel Boundary Fault are very similar and expected to be of interest not only for the Roer Valley Rift System and Lower Rhine Embayment (Fig. 1), but also for other rift systems in unconsolidated (soft) sediments. However, only very few studies (e.g., Balsamo and Storti 2010) consider the implications of fault permeability on cross-fault groundwater flow. In addition, also the multiyear and high-frequency monitoring of groundwater levels in a dense cross-fault monitoring network in unconsolidated (soft) sediments presented in this work, is unique. Based on the overall results, new insights are given to improve near-fault groundwater models. Thus far, these models often use permeability values inferred from model calibration instead of in situ measurements, and temporal and spatial variability of cross-fault groundwater levels are not taken into account (Lapperre et al. 2019). The results are also used to discuss the possible effects of climate change on future phreatic cross-fault groundwater levels and opportunities for fault-related water conservation and nature restoration.

## Setting

### Geology and geomorphology

The Roer Valley Graben (RVG) forms the central part of the Roer Valley Rift System and is bound by the Feldbiss Fault

**Fig. 1** The Feldbiss Fault zone (FFZ), Roer Valley Graben (RVG), Peel Boundary Fault zone (PBFZ), Tegelen Fault zone (TFZ) and study area near Bakel (B) in the Roer Valley Rift System (RVRS) as the northwestern continuation of the Lower Rhine Embayment (LRE). Coordinate system is in latitude-longitude using UTM projection. Modified from Van Balen et al. 2019
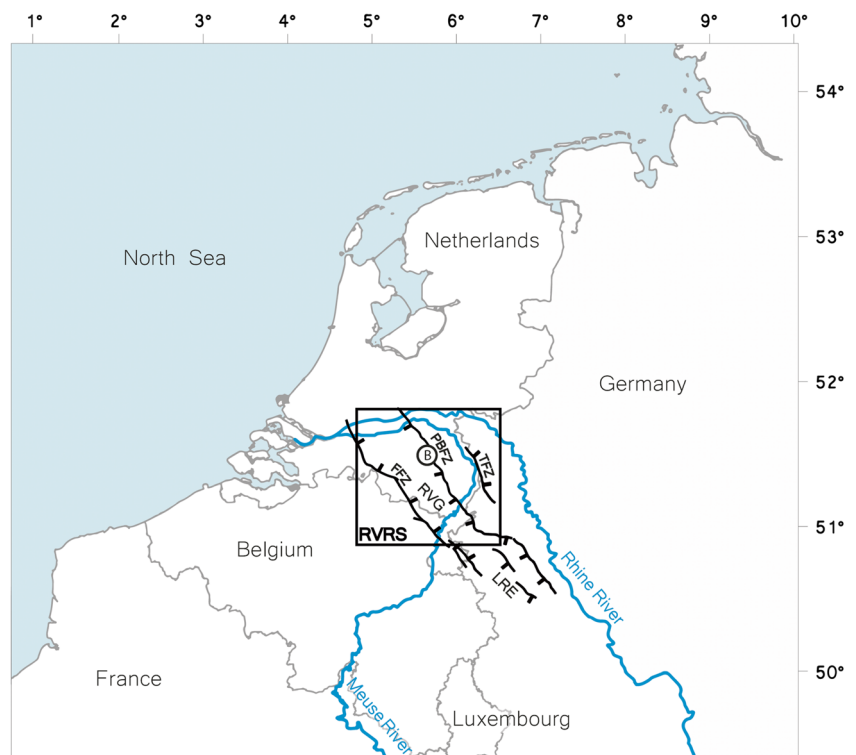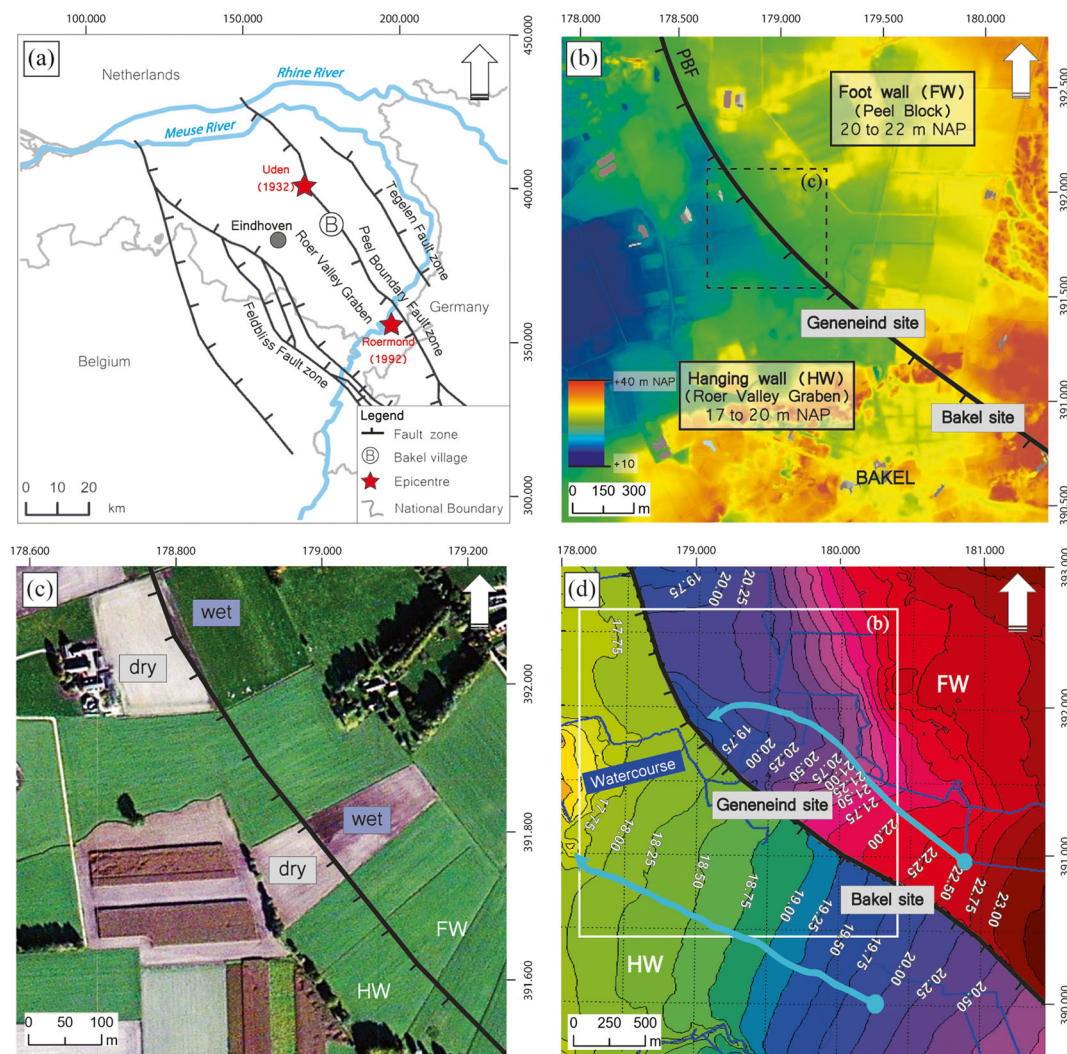
**Fig. 2** Location of the Bakel site, Geneneind site and overview figures. Coordinate system is the Dutch 87 National Grid (RD). **a** B indicates the village of Bakel, and the red star shows the epicentres of earthquakes in 1932 and 1992 related to faults of the Peel Boundary Fault zone (PBFZ); **b** digital elevation model based on AHN3 (2019) showing levels with respect to the Dutch Ordnance Datum (NAP) indicating the location of the Bakel and Geneneind sites at a fault (PBF) of the PBFZ; **c** crop marks and soil moisture contrasts on a satellite image indicating the exact location of the fault, between the wet foot wall (FW) and the drier hanging wall (HW) agricultural plots and **d** overview of the regional isohypses pattern (groundwater level contours) on 1 April 2016 (m NAP), with the fault modelled as an (almost) impermeable boundary, and corresponding groundwater flow path (blue arrows) at both sides of the fault using the regional groundwater model GRAM2.0 from water authority Aa en Maas. The position of part **b** is indicated in **d** and part **c** is indicated in **b**

zone in the southwest and by the PBFZ in the northeast (Fig. 1). The current phase of extension of the RVG started during the late Oligocene (Michon et al. 2003; Michon and Van Balen 2005; Van Balen et al. 2005). In 1843 ($M_L$ 4.8) and in 1932 ($M_L$ 5.0), earthquakes took place in Uden and in 1992 a moderate earthquake took place near Roermond ($M_L$ 5.8). These earthquakes originated along the PBFZ (Fig. 2a).

Faults of the PBFZ are geomorphologically visible in the field as a series of northwest–southeast-oriented fault scarps with a height of several metres in many places. In the study area, the scarp height of the fault varies from 0.5 to 1 m, but locally Holocene drift-sand dunes are present with steeper slopes and larger elevation differences of around 2–4 m.

Due to cultivation, the scarp height has decreased to a more gradual slope (Fig. 2b) over the past centuries. Locally, crop marks and sharp transitions from dark-coloured wet soils (reflecting shallow groundwater levels on the foot wall) to light-coloured dry soils (deep groundwater levels on the hanging wall) reveal the trace of the fault (Fig. 2c).

The Bakel site was excavated and studied in the fall of 2014 to document stratigraphy of the shallow subsurface, the fault-induced displacement and the paleoseismic activity (Van Balen et al. 2019). Prior to excavation the approximate location of the Peel Boundary Fault (PBF) was determined using the groundwater-level step (Fig. 2d) located through drilling. Because of deeper groundwater levels on the hanging

wall (Roer Valley Graben) excavation was possible to a maximum depth of 3.7 m.

In contrast, shallow groundwater levels on the foot wall (Peel Block) allowed for initial excavation of ~2 m. Subsequently, groundwater pumping was required to allow a deepening of this side of the trench by another 2 m. The trench revealed unconsolidated sediments only (Fig. 3). The lowermost deposits on the foot wall (Fig. 3a) consisted of coarse sand with gravel (unit A) deposited by the Meuse River system (Van Balen et al. 2019). These fluvial sediments were covered by (partly reworked) aeolian deposits of sandy loam and loamy sand of Weichselian Early Late Glacial age, with a maximum thickness of 1 m (unit B). On top of these aeolian deposits, and on the hanging wall only, a colluvial wedge of gravelly sands was found (unit C). The presence of this particular unit (Fig. 3c) is related to fault-scarp erosion and deposition on the hanging wall (Van Balen et al. 2019). The scarp geomorphology in the Bakel trench was blanketed with aeolian deposits known as coversands (unit D), with an intercalated soil (the Usselo Soil of Allerød age; Kasse et al. 2007; Van Balen et al. 2019). A Holocene podzol soil, often disturbed by human activity, has developed at the surface. The trench also revealed the subvertical, approximately 1-m-wide fault zone with faults and cracks (Fig. 3b). The displacement of both the top and the base of the greyish sandy loam and loamy sand layer (unit B) in the fault zone was 1.15 m. Based on optically stimulated luminescence (OSL) dating (Rhodes 2011), most of this fault-induced displacement occurred around 14 ka (Van Balen et al. 2019). A prominent clastic dyke is present in the fault zone (Fig. 3). This fluid-escape structure consists of loamy fine sand and intruded the fault zone by an upward injection of fine sediments from below the trench floor (Van Balen et al. 2019). Such fluidization structures arise in unconsolidated sediments in water-saturated conditions during seismic shaking (Vanneste et al. 1999; Bokanda et al. 2018).

## Hydrology

The regional and local groundwater and surface-water system near Bakel is substantially influenced by the presence of the Peel Boundary Fault (Fig. 2c,d). The regional phreatic groundwater levels on the Peel Block are systematically higher compared to the levels in the Roer Valley Graben (Bense et al. 2003a; Bense et al. 2016, Lapperre et al. 2019). On this regional scale, the groundwater-level isohypses (groundwater-level contours) at both sides of the fault zone indicate a southeast–northwest groundwater-flow direction almost parallel to the fault (Fig. 2d). The isohypses pattern also indicates interaction between surface water and groundwater: watercourses on the foot wall mostly drain the shallow groundwater system, while the water courses on the hanging wall often infiltrate and replenish the groundwater system. At

the Bakel and Geneneind sites, the flow direction of the phreatic groundwater is not perfectly parallel to the fault, probably indicating that the Peel Boundary Fault is not impermeable, but has low permeability. Model calculations with the calibrated regional groundwater model (GRAM2.0) from water authority Aa en Maas, based on validated groundwater level measurements, resulted in phreatic cross-fault groundwater levels that vary from 2.5 m in the southeast to around 2 m in the northwest. At the Bakel site, the model-calculated step on 1 April 2016 was around 2.6 m (Fig. 2d).

## Methods

The Bakel and Geneneind sites are located in a similar geological and geomorphological setting and both monitoring arrays are situated across the same fault of the PBFZ (Fig. 4a). The layout of both sites in terms of filter depth, perforated filter length, filter diameter and use of automated data loggers is similar. Monitoring of cross-fault groundwater levels took place during the same monitoring period (13 January 2015 to 10 February 2020), with the same frequency (every hour) and an identical data validation process for both sites was performed.

### Bakel site

The monitoring network at the Bakel site (Fig. 4b) was completed in early 2015 after full repair of the trench in December 2014 when the original structure of the subsoil was restored as accurately as possible and the excavated fault zone was filled with low-permeability (sandy) loam. To measure the possible effect of renewed precipitation of minerals such as iron (hydro)oxides on fault-zone hydrogeology, a frame with an area of 1 $m^2$ (Fig. 4c) filled with sand was placed in the fault zone at a depth of 2.2 m below ground surface. This frame (Fig. 4d) was positioned according to the dip direction and dip angle in the middle part of the fault as described by Van Balen et al. (2019).

A total of 11 phreatic piezometers (numbered 1–8 and 4A–4C) have been installed, varying in depth from 3.04 to 5.77 m below ground surface (Fig. 4b). Six piezometers (numbered 1–6) are positioned in an almost straight line and equally distributed over the foot wall (numbers 1–3) and hanging wall (numbers 4–6). The monitoring array has a length of 103 m and runs (almost) perpendicular across the Peel Boundary fault. Piezometers 7 and 8 are positioned on the foot wall parallel to the fault. They are 36 m apart. Piezometers 4A–4C were placed in February 2021 to measure the possible effect of permeability reduction after a monitoring period of 5 years (2015–2020). These piezometers were added to study the possible effects of renewed iron precipitation on a small (1 $m^2$) section of the fault (Fig. 4c) where the frame filled with
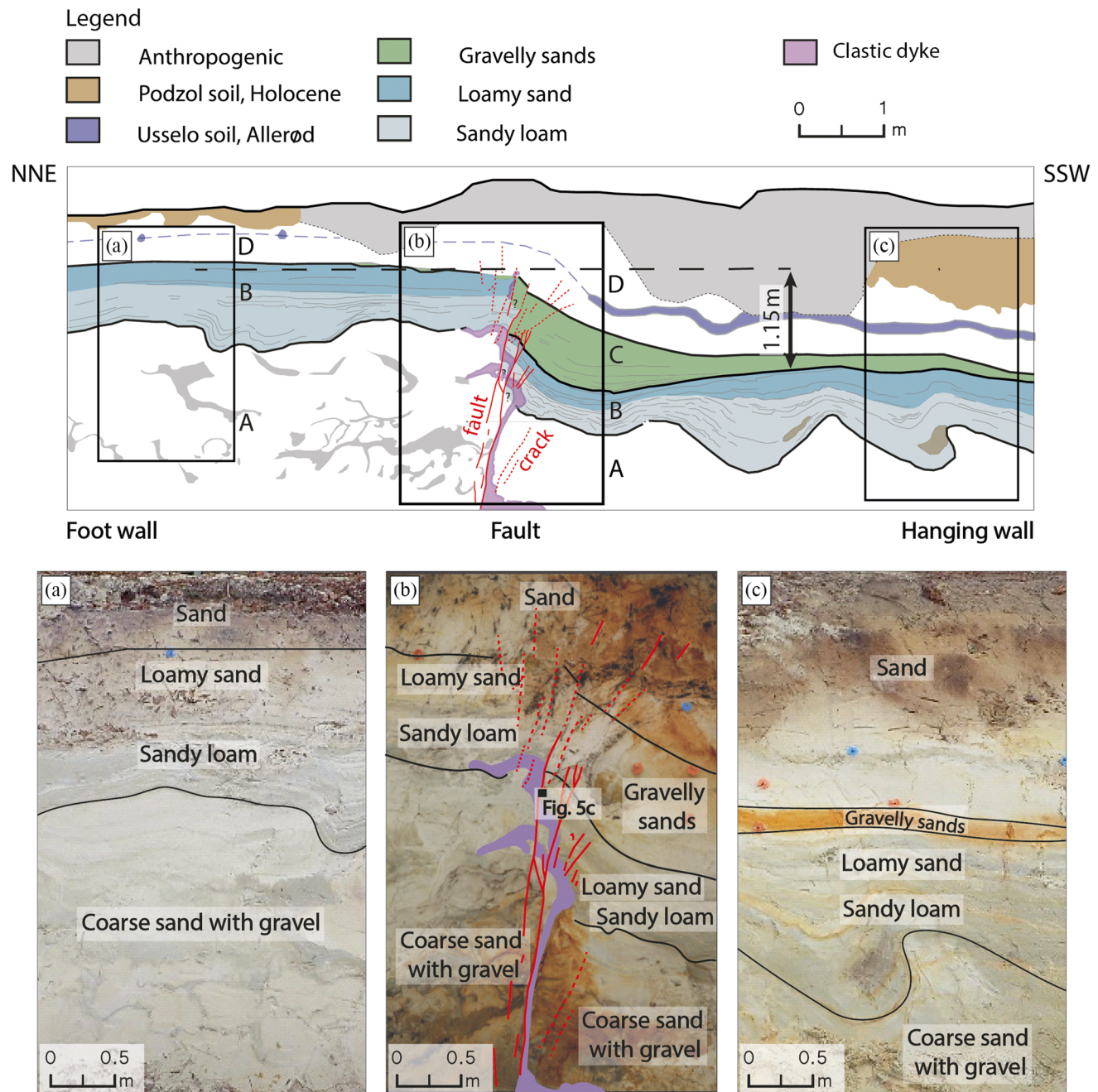
**Fig. 3** Cross-section of the Bakel trench with a fault-induced displacement of 1.15 m and documented stratigraphy (modified from Van Balen et al. 2019). **a** detail of the lithostratigraphy of the foot wall with sandy loam and loamy sand (unit B) and aeolian coversands (unit D) on top of coarse sand with gravel (unit A); **b** detail of the fault with the subvertical clastic dyke (purple colour) and adjoining faults and cracks and displacement of the sandy loam and loamy sand layers (unit B) and **c** detail of the lithostratigraphy of the hanging wall with the orange coloured colluvial wedge (unit C) with gravelly sands in between finer sediments. Orange coloured bands (**b** and **c**) are related to precipitation of minerals such as iron (hydro)oxides under oxic conditions

sand was placed (Fig. 4d). The diameter of all piezometers varies from 32 to 60 mm and the perforated filter length is 1 m. To allow for reliable and frequent measurements of groundwater levels all piezometers were either placed outside the excavation or below the trench floor in undisturbed sediments and equipped with data loggers (Mini-Diver® DI501)

for automatic groundwater level recording. Table 1 presents the layout of the Bakel site.

The data loggers in piezometers 1, 2, 3, 4, 5, 7 and 8 have been measuring groundwater levels every hour since 13 February 2015. The data logger in piezometer 6 has been active since 7 March 2015 and the loggers in piezometers
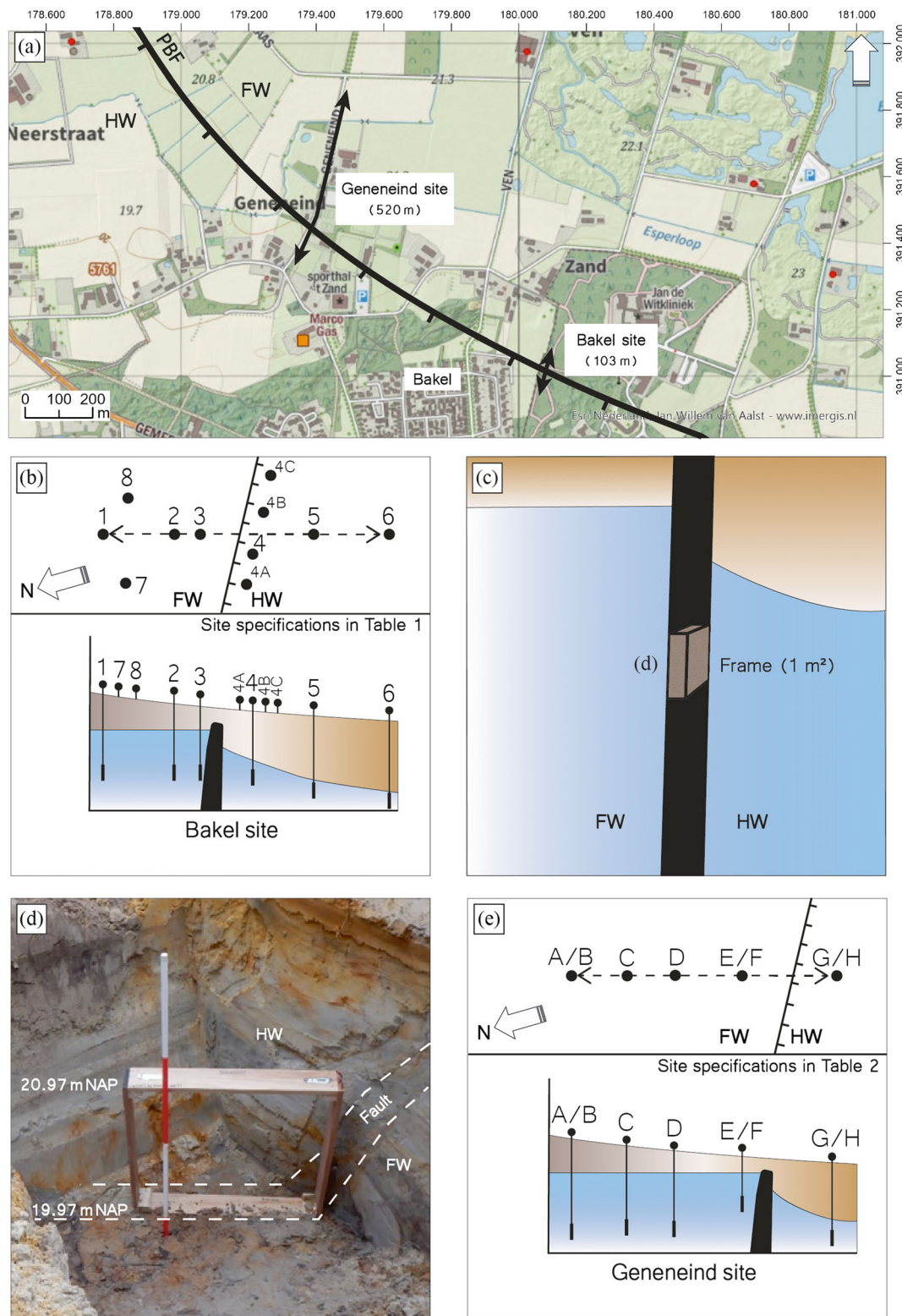
Fig. 4 Bakel and Geneneind sites at the Peel Boundary Fault (PBF). The coordinate system is the Dutch 87 National Grid (RD) and levels are with respect to the Dutch Ordnance Datum (NAP). a Location of the Bakel and Geneneind sites; b top view and cross-section of the Bakel site (site layout in Table 1) with piezometers 1, 2, 3, 7 and 8 on the foot wall (FW) and piezometers 4–6 and 4A–4C on the hanging wall (HW), where blue is the saturated and brown the unsaturated zone; c artists' impression of the position of the frame in the fault; d installation of the frame just before filling with low-permeability (sandy) loam and e top view and cross-section of the Geneneind site (site layout in Table 2) with piezometers A–F (FW) and piezometers G–H (HW)

**Table 1** Locations, surface elevations and piezometer layout at the Bakel site (Fig. 4a–d)

| Piezometer/frame | | Coordinate[a] | | Surface elevation (m NAP)[b] | Piezometer length (m bgs)[c] | Piezometer end depth (m NAP) | Filter length (m) | Piezometer diameter (mm) |
|---|---|---|---|---|---|---|---|---|
| (number) | (local field code) | (X) | (Y) | | | | | |
| 1 | BRBA01_G | 180,072.400 | 391,022.085 | 23.07 | 4.72 | 18.35 | Unknown | 40 |
| 2 | BRBA02_G | 180,066.016 | 390,998.728 | 22.27 | 5.45 | 16.82 | Unknown | 60 |
| 3 | BRBA03_G | 180,062.645 | 390,995.480 | 22.19 | 3.04 | 19.15 | 1.00 | 32 |
| 4 | BRBA04_G | 180,059.754 | 390,991.729 | 22.19 | 3.13 | 19.06 | 1.00 | 32 |
| 4A | BRBA04A_G | 180,057.932 | 390,995.047 | 22.46 | 3.45 | 19.01 | 1.00 | 32 |
| 4B | BRBA04B_G | 180,062.991 | 390,988.161 | 22.39 | 3.11 | 19.28 | 1.00 | 32 |
| 4C | BRBA04C_G | 180,066.100 | 390,984.180 | 22.36 | 3.28 | 19.08 | 1.00 | 32 |
| 5 | BRBA05_G | 180,054.279 | 390,981.411 | 22.26 | 4.14 | 18.12 | 1.00 | 32 |
| 6 | BRBA06_G | 180,039.026 | 390,926.217 | 22.11 | 4.90 | 17.21 | 1.00 | 32 |
| 7 | BRBA07_G | 180,054.280 | 391,021.370 | 23.10 | 4.87 | 18.23 | 1.00 | 40 |
| 8 | BRBA08_G[d] | 180,088.774 | 391,004.649 | 23.09 | 5.77 | 17.32 | 1.00 | 60 |
| Frame[e] | West boundary | 180,061.085 | 390,994.148 | 22.17 | Top frame 20.97 m NAP | Bottom frame 19.97 m NAP | – | – |
| | East boundary | 180,061.754 | 390,993.354 | 22.17 | Top frame 20.97 m NAP | Bottom frame 19.97 m NAP | | |

[a] Coordinate system is the Dutch 87 National Grid (RD)

[b] Level with respect to the Dutch Ordnance Datum: Normaal Amsterdams Peil (NAP)

[c] Metre below ground surface

[d] Piezometer BRBA08_G is also equipped with a Baro-Diver®

[e] Frame area 1 $m^2$: filling material is sand

4A–4C since 6 February 2021. At piezometer 8, atmospheric air pressure is recorded and the elevation of the piezometers has been measured relative to NAP. Both, atmospheric air pressure variation and reference height are used in the data validation process.

## Geneneind site

The Geneneind site (Fig. 4a) is situated approximately 700 m northwest of the Bakel site. Here, eight piezometers (labelled A–H) are in a line 520 m long, crossing the fault perpendicular (Fig. 4e). All loggers have been active since 25 May 2015 and measure groundwater levels every hour. The phreatic piezometers vary in depth from 2.62 to 6.07 m below ground surface, have a perforated filter length of 1 m and a diameter of 32–50 mm. Table 2 presents the layout of the Geneneind site.

With the exception of piezometers A and H, the piezometers at the Geneneind site suffered from occasional failure of the data loggers. Because one or more data loggers were always operational on the foot wall and hanging wall, there are no monitoring gaps during the 2015–2020 period.

## Data validation and interpretation

Groundwater-level measurements from the Bakel and Geneneind sites have been validated with ArtDiver® software

from Artesia Water Research Unlimited, which uses four validation steps. During the first validation step, all groundwater-level measurements were corrected for variation in atmospheric air pressure measured with a Baro-Diver® installed at the Bakel site. From 9 April 2018, measurements could no longer be performed with the Baro-Diver® due to malfunction. Validated values from the Royal Dutch Meteorological Institute were used instead. This first step results in validated *relative* groundwater-level measurements in each piezometer. A second and third validation step were executed to convert relative into *absolute* groundwater levels with reference to NAP. In the second step the reference height and exact position of the data logger were therefore verified and in the third validation step the preliminary data were compared with manual verification measurements. These field checks are carried out three times a year. In the fourth and final validation step, the measurement series were corrected for sporadic errors due to equipment malfunction or reading errors. The final high-frequency measurement series have a relative accuracy of 2–3 cm between piezometers.

Computer program Menyanthes (Von Asmuth 2012) was applied to analyse the groundwater-level measurements (time series) for both sites. The methods used in Menyanthes are based on multiple predefined impulse response functions in continuous time (PIRFICT) and use precipitation and evapotranspiration (reference crop evapotranspiration), surface-

**Table 2** Locations, surface elevations and piezometer layout at the Geneneind site (Fig. 4a,e)

| Piezometer | | Coordinate[a] | | Surface elevation | Piezometer length | Piezometer end depth | Filter length | Piezometer diameter |
|---|---|---|---|---|---|---|---|---|
| (label) | (local field code) | (X) | (Y) | (m NAP)[b] | (m bgs)[c] | (m NAP) | (m) | (mm) |
| A | PEEL001_1_1 | 179,482.866 | 391,871.625 | 21.00 | 2.91 | 18.09 | 1.00 | 32 |
| B | PEEL001_1_2 | 179,482.841 | 391,871.600 | 21.00 | 4.54 | 16.46 | 1.00 | 50 |
| C | PEEL001_2_1 | 179,451.579 | 391,723.432 | 20.78 | 3.02 | 17.76 | 1.00 | 50 |
| D | PEEL001_3_1 | 179,424.415 | 391,564.258 | 20.77 | 4.59 | 16.18 | 1.00 | 50 |
| E | PEEL001_4_1 | 179,407.647 | 391,501.347 | 20.62 | 2.62 | 18.00 | 1.00 | 32 |
| F | PEEL001_4_2 | 179,407.622 | 391,501.322 | 20.62 | 3.82 | 16.80 | 1.00 | 50 |
| G | PEEL001_5_1 | 179,345.452 | 391,373.605 | 20.20 | 3.57 | 16.63 | 1.00 | 32 |
| H | PEEL001_5_2 | 179,345.427 | 391,373.580 | 20.20 | 6.07 | 14.13 | 1.00 | 50 |

[a] Dutch 87 National Grid (RD)

[b] Level with respect to the Dutch Ordnance Datum: Normaal Amsterdams Peil (NAP)

[c] Metres below ground surface

water levels and groundwater abstractions as explaining variables. For extrapolation of measured foot-wall and hanging-wall groundwater levels, towards the fault, the spline function from programming platform MATLAB (Higham and Higham 2017) was used.

## Meteorological data

Precipitation and evapotranspiration control groundwater-level variation (Gunduz and Simsek 2011; Zaadnoordijk et al. 2018). To analyse the groundwater measurement series, precipitation and evaporation data are used as collected by the Royal Dutch Meteorological Institute (KNMI) at nearby weather station Eindhoven (station 370). The precipitation values are accurate to within 0.1 mm for precipitation events up to 5 mm. For larger events the accuracy is 2% (KNMI 2000). Based on the 24-h sum of the global radiation and temperature, the daily reference crop evapotranspiration is calculated by the KNMI using the Makkink method (Elbers et al. 2009). The precision of this data is 0.1 mm (KNMI 2000).

For the analysis of the cross-fault groundwater-level-measurement series, 43,748 validated hourly precipitation values and 1,824 validated daily reference crop evapotranspiration values available from 13 January (6 pm) 2015 to 10 February (1 pm) 2020 are used.

## Fault-zone saturated conductivity measurements

In this paper *permeability* is used in a general sense to refer to the capacity of the subsurface to allow water to pass through, and *saturated hydraulic conductivity* is used when permeability is quantified, e.g., through measurements. The Netherlands Organisation for Applied Scientific Research (TNO) collected

12 undisturbed sediment samples from the Bakel trench. The samples had a volume of approximately 2,600 ml. They were collected in parallel (vertical) and perpendicular (horizontal) directions to the Peel Boundary Fault. After lithological description, a total of 25 laboratory samples were prepared and the saturated hydraulic conductivity measured using three different methods. Ten samples with an undisturbed standard soil volume of 100 ml and an expected saturated hydraulic conductivity of 0.01 m day$^{-1}$ or higher were measured at least twice using a permeameter (Eijkelkamp 2017 modified by TNO). When the outcome of the falling head measurements for a single sample were within a range of 10%, the final, average saturated hydraulic conductivity value $K_{sat}$ (m day$^{-1}$) was calculated. Fifteen samples with an expected saturated hydraulic conductivity less than 0.01 m day$^{-1}$ were measured using a modified oedometer or triaxial testing. Both test procedures for measuring low-permeability samples (NEN-EN-ISO 2019) were conducted in the geotechnical laboratory of the Deltares institute for applied research (Delft, the Netherlands). The oedometer test was applied for measuring saturated hydraulic conductivity for eight homogeneous low-permeability samples and the triaxial test for seven stratified low-permeability samples. The combined use of the three described measurement methods has resulted in 25 saturated hydraulic conductivity values for the Bakel site.

## Results

### Variation in fault-zone hydraulic conductivity

The 25 measured saturated hydraulic conductivity values at the Bakel site are presented in Table 3. They are based on fault

and near-fault samples from undisturbed sediments and collected both in the horizontal direction (five field samples) and in the vertical direction (seven field samples) in the trench across the fault (Fig. 5a). The table also provides details on sampling location, stratigraphic unit, lithology and conductivity direction.

The saturated hydraulic conductivity values vary from 0.003 to 4.43 m day$^{-1}$. The results show conductivity variation up to 3 orders of magnitude and are in agreement with expectations based on the lithology of the sediments (Lapperre et al. 1996; Taheri et al. 2017). Relatively coarser sediments such as medium fine, gravely sand and very fine sand (samples 4 and 19) generally show higher saturated conductivity values (3.60 and 2.06 m day$^{-1}$) than finer deposits such as sandy loam and loamy sand (samples 16 and 22) with values of 0.005 and 0.11 m day$^{-1}$ respectively. Since most of the samples contained a mixture of coarser and finer deposits, the majority of the saturated hydraulic conductivity values range between 0.04 and 1.90 m day$^{-1}$.

The results of 13 horizontally oriented samples show an average saturated hydraulic conductivity value of 0.53 m day$^{-1}$ (range: 0.02–4.43 m day$^{-1}$). This is on average one order of magnitude higher than the average value from 12 vertical samples, showing an average value of 0.05 m day$^{-1}$ (range: 0.003–2.73 m day$^{-1}$). The clastic dyke in the fault core was sampled three times (samples 3, 5 and 25). The saturated hydraulic conductivity values range from 0.02 m day$^{-1}$ (Fig. 5b) to 0.47 m day$^{-1}$ (Table 3). Two box cores from the fault core (Fig. 5c,d) were collected to study the effect of fault displacement on lithological composition. The first box core (Fig. 5c) reveals the characteristic subvertical orientation of the clastic dyke which has a sedimentary composition of loamy fine sand. The measured low horizontal hydraulic conductivity values are consistent with the fine-grained nature and moderate sorting of the clastic dyke relative to the surrounding host sediments. Permeability reduction is further enhanced by the loss of the original horizontal layering and the presence of alongside sediments with an abrupt decrease in grain size distribution. The second box core from the fault core (Fig. 5d) shows faulted layers. As a result, layers with various composition and different hydraulic properties are juxtaposed. This also contributed to a reduced conductivity perpendicular to the fault.

## Groundwater levels and cross-fault variation

The 2015–2020 groundwater-level time series from the Bakel and Geneneind sites reveal characteristic hydrological differences between the groundwater system in the foot wall and in the hanging wall, e.g., showing cross-fault groundwater-level differences that vary spatio-temporally.

### Bakel site

The highest phreatic groundwater levels at the Bakel site are recorded *on the foot wall*. Piezometers 1 and 2 show average levels of 20.90 m NAP, piezometer 3 an average level of 20.89 m, and piezometers 7 and 8 average levels of 20.89 and 20.92 m NAP respectively. The recorded levels in these five foot-wall piezometers (Fig. 5a) are further characterized by relatively small and spiky, temporal variations (Fig. 6) compared to the variations on the hanging wall (Fig. 7). The range of groundwater-level variations on the foot wall generally (90% of the time) do not exceed 0.63 m. The seasonal variation has an amplitude of 0.3 m around the average phreatic groundwater level (Fig. 6). Lower levels are usually recorded during summer and early autumn (July–August–September) and higher levels during winter and early spring (January–February–March). The peak level in June 2016 (Fig. 6) is an exception and caused by abundant precipitation in a short period of time.

Groundwater levels *on the hanging wall* are lower than on the foot wall. The level drops with increasing distance from the fault into the hanging wall (Fig. 7). The average phreatic groundwater level on the hanging wall varies from 20.43 m NAP (piezometer 4) via 18.91 m NAP (piezometer 5) to 18.59 m NAP (piezometer 6). The results of piezometer 4 (Fig. 6), on the hanging wall, just next to the fault, show a spiky pattern and groundwater-level variation (0.78 m) resembling the groundwater-level variation on the foot wall (piezometers 1, 2, 3, 7 and 8). However, phreatic groundwater levels in piezometer 4 are on average 0.46 m lower than in piezometer 3 on the foot wall. Thus, the results from piezometer 4 resemble the piezometer results from both the foot wall and the hanging wall (Fig. 7). This also applies to the results from piezometers 4A–4C (Fig. 5a). Multiple measurements in February and March 2021 revealed small groundwater-level differences between the phreatic groundwater level in near-frame piezometer 4 and the three nonframe-piezometers 4A–4C. The recorded levels in 4A were 0.10 m higher than levels in piezometer 4, while levels in 4B and 4C were 0.15 and 0.25 m lower respectively. Based on these small differences it is concluded that the time series from piezometer 4 is characteristic of the near-fault hanging-wall groundwater levels and is not significantly affected by the presence of the frame. Apparently, the 5-year time period was too short for significant iron (hydro)oxide precipitation. To study the effects over a longer period of time, the frame (Fig. 4c) and piezometers (Fig. 4b) remain in place and monitoring is continued.

Piezometers 5 and 6 reveal a different hydrological regime in which the phreatic groundwater level fluctuates more gradually over time. This suggests a much more rapid response in groundwater levels with distance closer to the fault and a more delayed response with distance further away from the fault.

**Table 3** Variation in average saturated hydraulic conductivity value ($K_{sat}$) at the Bakel site

| Conductivity sample | DINOloket TNO[a] | Coordinate[b] field samples | Trench sample location | Trench sample depth | Stratigraphic unit | Lithology general description | Measuring method | Average saturated hydraulic conductivity value ($K_{sat}$) | Hydraulic conductivity direction |
|---|---|---|---|---|---|---|---|---|---|
| (number) | (national field code) | (X and Y) | (trench code) | (m NAP)[c] | (Fig. 3) | (NEN 5104)[d] | (–) | (m day$^{-1}$ at 10 °C) | (–) |
| 1 | B52A1509 | 180062.650 390983.500 | BA-01 | 21.00–20.67 (vertical sample) | Unit D (hanging wall) | Very fine sand, moderately silty, few loam laminae | Permeameter[e] | 0.86 | Horizontal |
| 2 | B52A1509 | 180062.650 390983.500 | BA-01 | 21.00–20.67 (vertical sample) | Unit D (hanging wall) | Very fine sand, slightly silty, loamy laminae, iron precipitation (diffuse) | Permeameter | 0.04 | Vertical |
| 3 | B52A1510 | 180061.700 390990.600 | BA-02 | 20.50 (horizontal sample) | Clastic dyke (fault zone) | Loamy fine sand | Modified oedometer[f] | 0.02 (Fig. 5b) | Horizontal |
| 4 | B52A1511 | 180061.700 390990.600 | BA-02 | 20.50 (horizontal sample) | Unit C (hanging wall) | Medium fine, gravelly sand, iron precipitation | Permeameter | 3.60 (Fig. 5b) | Horizontal |
| 5 | B52A1512 | 180061.850 390990.400 | BA-03 | 20.50 (horizontal sample) | Unit A and clastic dyke (fault zone) | Mixture of medium fine and medium coarse gravelly sand and loamy sand (sandy loam), iron precipitation (diffuse) | Triaxial[f] | 0.47 | Horizontal |
| 6 | B52A1514 | 180062.000 390990.150 | BA-04 | 20.50 (horizontal sample) | Unit unidentified (fault zone) | Loamy sand | Modified oedometer | 0.16 | Horizontal |
| 7 | B52A1515 | 180062.000 390990.150 | BA-04 | 20.50 (horizontal sample) | Unit C (hanging wall) | Medium fine sand, few gravel, diffuse iron precipitation | Permeameter | 0.53 | Horizontal |
| 8 | B52A1516 | 180063.300 390999.900 | BA-05 | 21.75–21.42 (vertical sample) | Unit B (foot wall) | Very fine sand, slightly silty, weakly laminated | Triaxial | 0.07 | Vertical |
| 9 | B52A1516 | 180063.300 390999.900 | BA-05 | 21.75–21.42 (vertical sample) | Unit B (foot wall) | Sandy loam, strongly laminated | Triaxial | 0.08 | Vertical |
| 10 | B52A1517 | 180065.400 391994.950 | BA-06 | 21.15–20.81 (vertical sample) | Unit B (foot wall) | Medium fine sand, moderately silty, little iron precipitation (diffuse) | Permeameter | 4.43 | Horizontal |
| 11 | B52A1517 | 180065.400 391994.950 | BA-06 | 21.15–20.81 (vertical sample) | Unit B (foot wall) | Very fine sand, slightly silty, little iron precipitation (diffuse) | Permeameter | 1.94 | Horizontal |
| 12 | B52A1517 | 180065.400 391994.950 | BA-06 | 21.15–20.81 (vertical sample) | Unit B (foot wall) | Very fine sand, slightly silty, little iron precipitation (diffuse) | Permeameter | 2.73 | Vertical |
| 13 | B52A1518 | 180071.350 391018.300 | BA-07 | 21.10–20.78 (vertical sample) | Unit B (foot wall) | Loamy sand, centimetre layering | Triaxial | 0.003 | Vertical |
| 14 | B52A1518 | 180071.350 391018.300 | BA-07 | 21.10–20.78 (vertical sample) | Unit B (foot wall) | Sandy loam, centimetre layering | Modified oedometer | 0.09 | Vertical |
| 15 | B52A1518 | 180071.350 391018.300 | BA-07 | 21.10–20.78 (vertical sample) | Unit B (foot wall) | Sandy loam, millimetre layering | Modified oedometer | 0.003 | Vertical |
| 16 | B52A1519 | 180071.300 391018.700 | BA-08 | 21.27–20.92 (vertical sample) | Unit B (foot wall) | Sandy loam, millimetre layering | Modified oedometer | 0.005 | Vertical |
| 17 | B52A1519 | 180071.300 391018.700 | BA-08 | 21.27–20.92 (vertical sample) | Unit B (foot wall) | Sandy loam, weakly laminated | Modified oedometer | 0.05 | Vertical |

**Table 3** (continued)

| Conductivity sample | DINO*loket* TNO[a] | Coordinate[b] field samples | Trench sample location | Trench sample depth | Stratigraphic unit | Lithology general description | Measuring method | Average saturated hydraulic conductivity value ($K_{sat}$) (m day$^{-1}$ at 10 °C) | Hydraulic conductivity direction |
|---|---|---|---|---|---|---|---|---|---|
| (number) | (national field code) | (X and Y) | (trench code) | (m NAP)[c] | (Fig. 3) | (NEN 5104)[d] | (–) | | (–) |
| 18 | B52A1519 | 180071.300 391018.700 | BA-08 | 21.27–20.92 (vertical sample) | Unit B (foot wall) | Sandy loam, cross lamination | Modified oedometer | 0.05 | Vertical |
| 19 | B52A1520 | 180057.950 390983.500 | BA-09 | 21.55–21.21 (vertical sample) | Unit B (hanging wall) | Very fine sand, slightly silty, millimetre aminae, diffuse iron precipitation | Permeameter | 2.06 | Horizontal |
| 20 | B52A1521 | 180058.400 390983.300 | BA-10 | 21.10–20.77 (vertical sample) | Unit B (hanging wall) | Sandy loam, centimetre layering | Permeameter | 0.11 | Vertical |
| 21 | B52A1521 | 180058.400 390983.300 | BA-10 | 21.10–20.77 (vertical sample) | Unit B (hanging wall) | Moderately fine sand, slightly silty, centimetre layering, iron precipitation (diffuse) | Triaxial | 0.05 | Vertical |
| 22 | B52A1522 | 180061.400 390990.000 | BA-11 | 20.55 (horizontal sample) | Unit B (fault zone) | Loamy sand, diffuse iron precipitation | Modified oedometer | 0.11 | Horizontal |
| 23 | B52A1523 | 180061.400 390990.000 | BA-11 | 20.55 (horizontal sample) | Unit B (fault zone) | Loamy sand, diffuse iron precipitation | Triaxial | 0.04 | Horizontal |
| 24 | B52A1524 | 180061.600 390990.500 | BA-12 | 20.65 (horizontal sample) | Unit B (fault zone) | Medium fine sand, diffuse iron precipitation, traces of organic matter | Permeameter | 1.07 | Horizontal |
| 25 | B52A1524 | 180061.600 390990.500 | BA-12 | 20.65 (horizontal sample) | Clastic dyke (fault zone) | Loamy sand (sandy loam), little iron, precipitation (diffuse) | Triaxial | 0.12 | Horizontal |

[a] The Netherlands Organisation for applied scientific research

[b] Dutch 87 National Grid (RD)

[c] Level with respect to the Dutch Ordnance Datum: Normaal Amsterdams Peil (NAP)

[d] Royal Netherlands Standardization Institute: 5104 (Dutch Soil Classification System)

[e] Measured by the Netherlands Organisation for applied scientific research
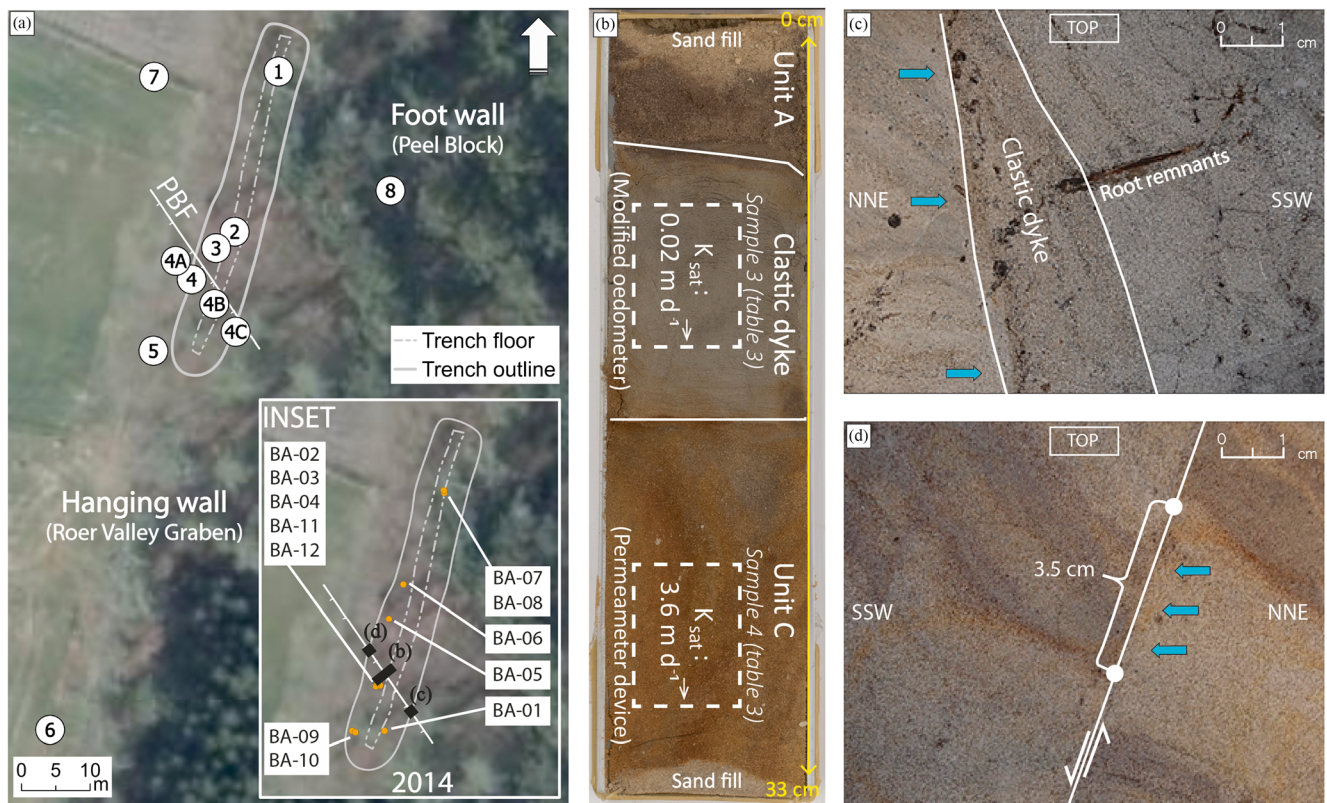
[f] Measured by Deltares Institute for applied research

**Fig. 5 a** Layout of the Bakel site, location of the Peel Boundary Fault (PBF), position of the 11 piezometers and refilled (2014) trench contour. The locations of all (near) fault conductivity trench samples BA-01 to BA-12 (details in Table 3) and box cores are shown in the inset; **b** trench sample BA-02 with horizontal conductivity sample 3 in the clastic dyke and conductivity sample 4 in unit C; **c** photograph of the box core sample of the clastic dyke in the fault core (vertical cross-section) and **d** photograph of box core sample of faulted layering in the fault core (vertical cross-section). Blue arrows indicate the predominant groundwater flow direction towards the fault derived from the available groundwater-level time series. White arrows indicate fault displacement direction
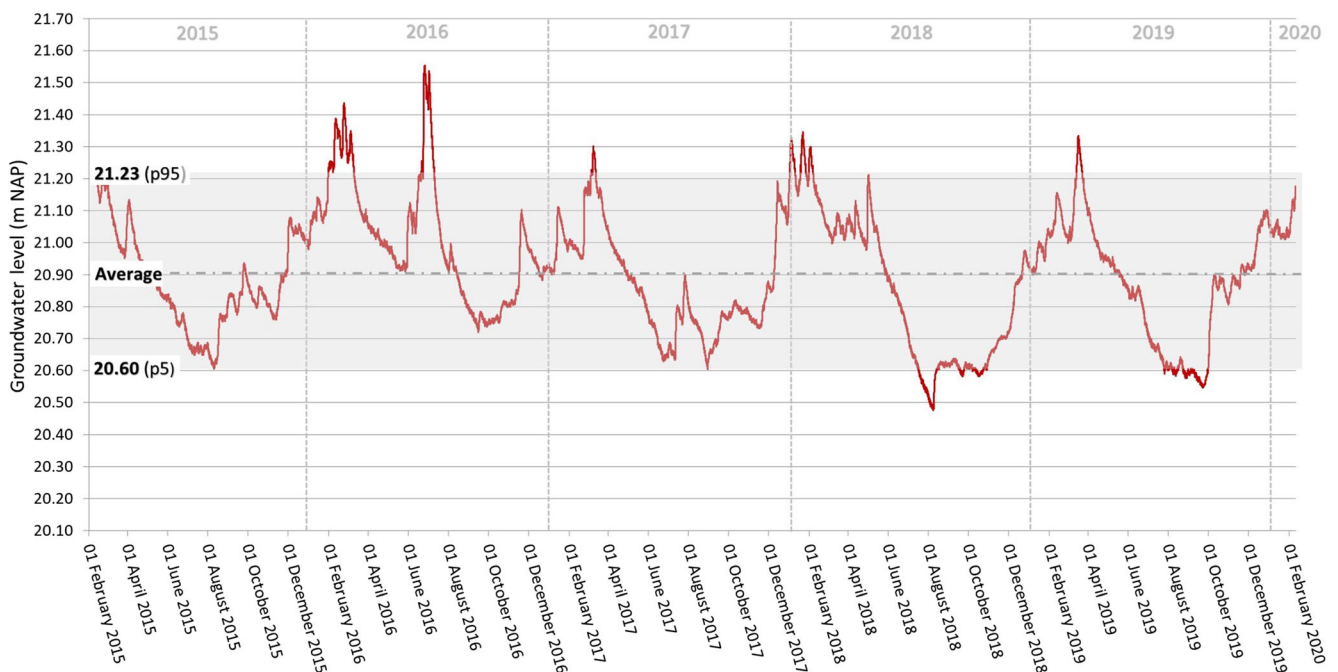


**Fig. 6** Phreatic groundwater-level variation (average from piezometers 1, 2, 3, 7 and 8) on the foot wall at the Bakel site (2015–2020; piezometer layout in Table 1). The shaded area shows a level range of 0.63 m that occurs during 90% of the monitoring period and ranges from 20.60 m NAP (p5) to 21.23 m NAP (p95). The dashed line marks the average phreatic groundwater-level of 20.90 m NAP
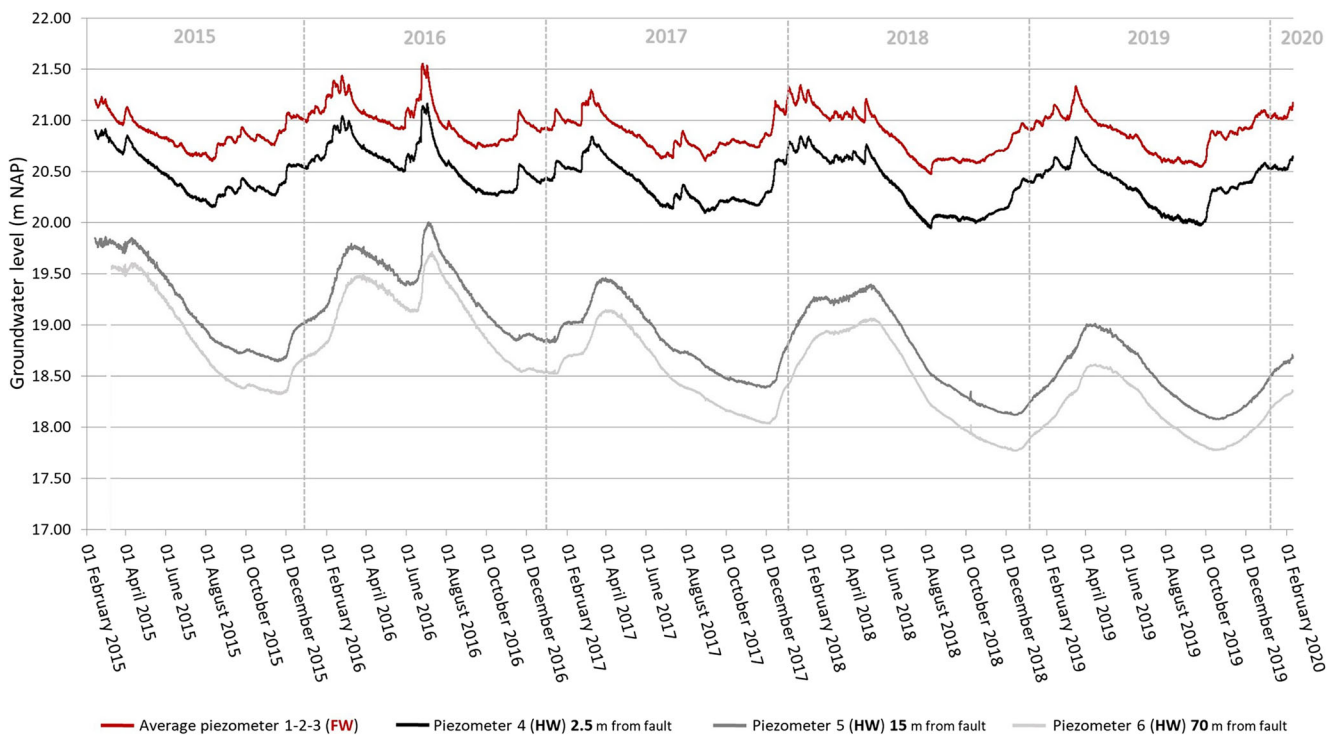
**Fig. 7** Phreatic groundwater-level variation on the foot wall (FW, red line) at the Bakel site (2015–2020) compared to the phreatic level variation on the hanging wall (HW, black and grey lines) taking into account the distance from the measuring points to the fault. Phreatic groundwater levels on the foot wall are the highest and show limited variation (details explained in Fig. 6). On the hanging wall, piezometers 4, 5 and 6 show permanently lower phreatic groundwater levels, and with increasing distance away from the fault (2.5, 15 and 70 m) levels further drop, to reveal a wider level range and levels that change more gradually

The level in piezometer 6 is on average 0.32 m lower than in piezometer 5 and on average 1.84 m lower than in piezometer 4 (Fig. 7).

Furthermore, the monitoring results in piezometers 5 and 6 show a (90% of the time) average phreatic groundwater-level variation of 1.61 and 1.65 m, respectively. This range is more than twice as large as the level variation (0.63 m) on the foot wall (Fig. 6). The phreatic groundwater levels on the hanging wall (piezometers 5 and 6) show a declining and repetitive pattern with seasonal peaks and troughs. The highest groundwater levels on the hanging wall are often measured in January–February–March, but with a delay of about 2 weeks compared to the foot wall. However, the lowest levels on the hanging wall are measured up to 2 or 3 months later, often around November–December, than the lowest levels on the foot wall.

### Geneneind site

The measurement results from the Geneneind site (Fig. 8a) also show an abrupt separation of the phreatic groundwater system at the fault. Between piezometers E/F and G/H (Fig. 4e) a cross-fault groundwater-level step is present. The levels on the foot wall are characterized by a limited variation—90% of the time they vary between 19.70 and 20.02 m NAP (range 0.32 m)—with an average phreatic water level of 19.88 m NAP. The level variation on the foot wall (piezometers A–F) and to some extent also piezometers G/H demonstrate a spiky pattern (Fig. 8a). Like at the Bakel site (Fig. 8b), hanging wall piezometers G/H show consistently lower phreatic groundwater levels (on average 18.49 m NAP), delayed peaks and troughs, and a wider level range (the average range, 90% of the time, is 1.63 m) with respect to the foot-wall water-level series. This groundwater-level variation almost equals the 90% variations measured at the Bakel site in piezometer 5 (1.61 m) and in piezometer 6 (1.65 m). At both sites (Fig. 8a,b), the highest levels on the hanging wall show a delay of approximately 2 weeks compared to the highest levels on the foot wall. The lowest levels on the hanging wall occur 2–3 months later than on the foot wall.

### Variation in cross-fault groundwater levels

At both sites, phreatic groundwater levels on the foot wall and hanging wall fluctuate, causing a variable phreatic cross-fault groundwater-level step. For the Bakel site an average step was calculated by comparing the average groundwater level from the foot wall (piezometers 1, 2, 3, 7 and 8) with the average
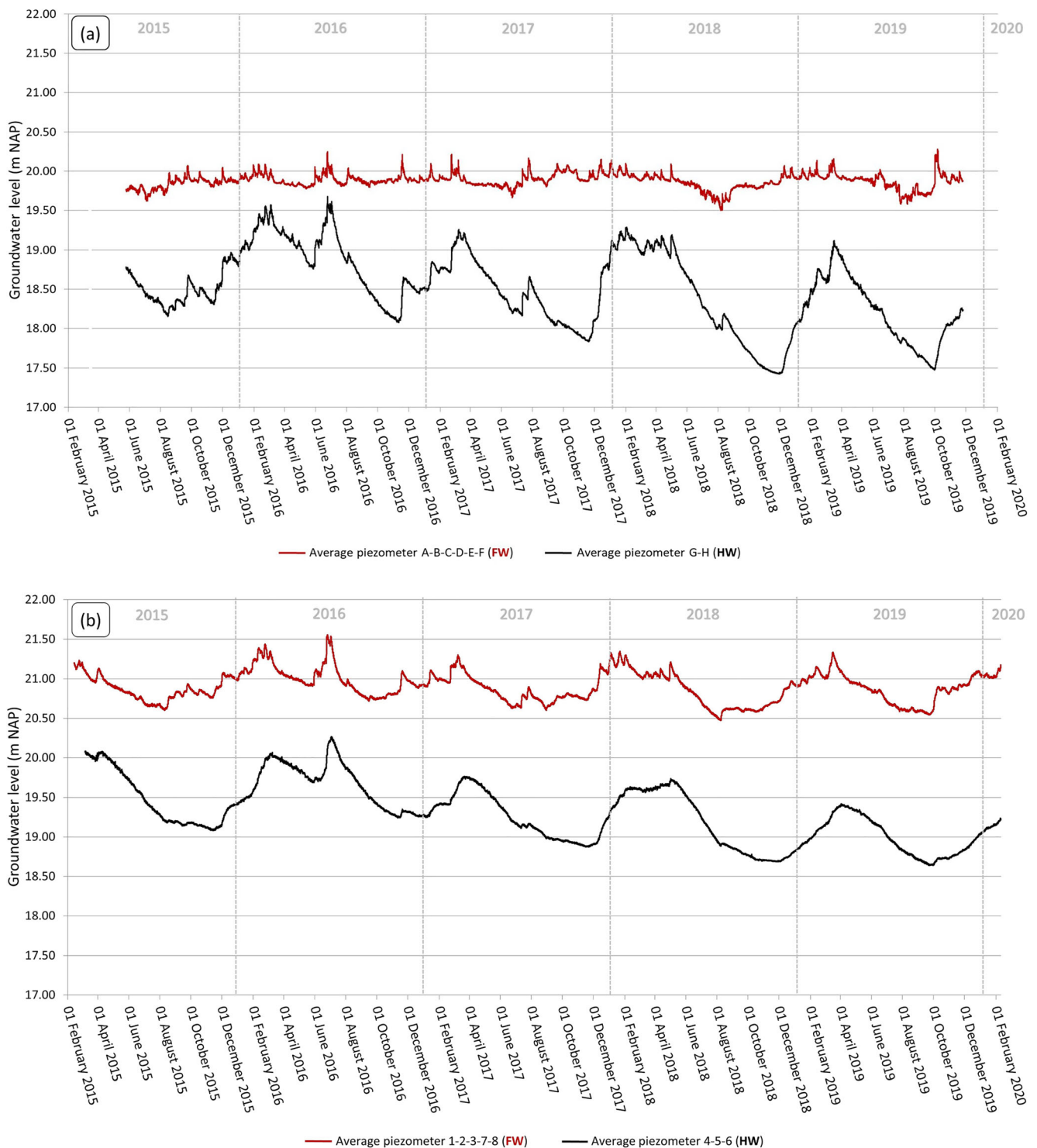
**Fig. 8** Groundwater levels at sites **a** Geneneind and **b** Bakel compared (2015–2020). Both sites show similar hydrological characteristics such as: a cross-fault groundwater-level step; high phreatic groundwater levels with a spiky pattern and shorter level range on the foot wall (FW, red lines), lower phreatic groundwater levels with a smoother pattern and wider level range on the hanging wall (HW, black lines); and a gradual decline of the phreatic water table on the hanging wall with a similar but delayed level variation pattern compared to the FW. A difference between the two sites is that the groundwater-level range on the HW of the Geneneind site is more spiky than the equivalent level variation pattern at the Bakel site
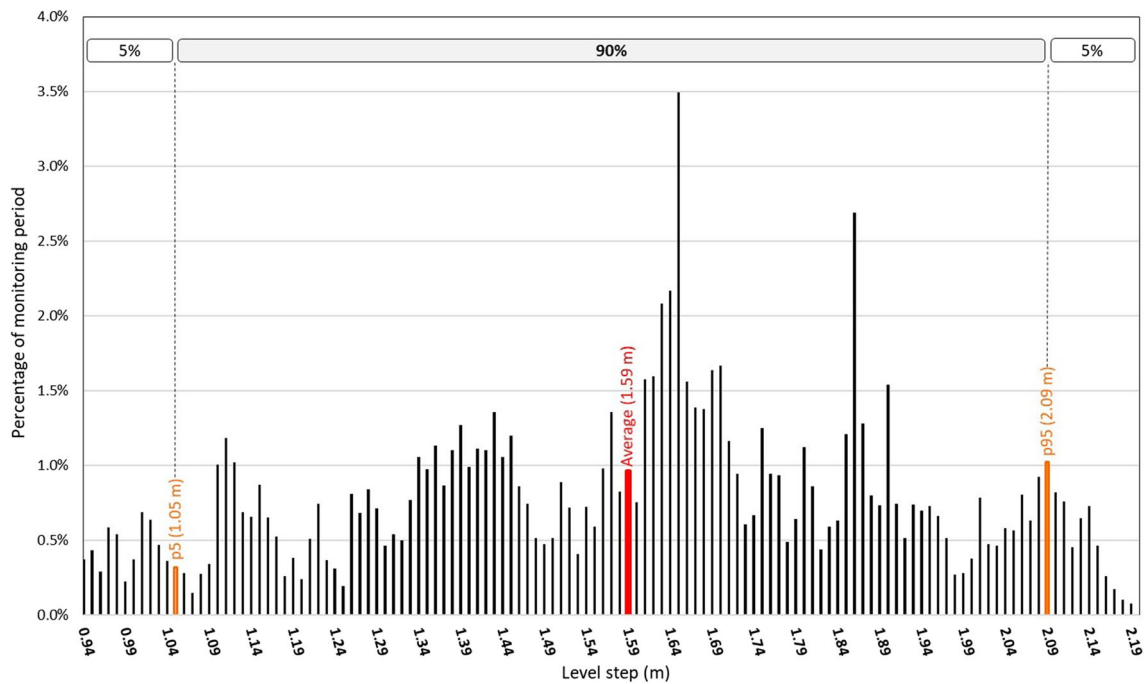
**Fig. 9** Range and distribution of the average phreatic cross-fault groundwater-level step at the Bakel site (2015–2020). The calculated range is 0.94–2.19 m. For 90% of the monitoring period the average cross-fault groundwater-level step varies from 1.05 (*p5*) to 2.09 (*p95*) m with an average of 1.59 m. Smaller (<1.05 m) or larger (>2.09 m) steps each occur 5% of the monitoring time

level on the hanging wall (piezometers 4-6). The approximately 43,000 measurements show an average phreatic cross-fault groundwater-level minimum and maximum of respectively 0.94 and 2.19 m (Fig. 9) with an average level of 1.59 m. For 90% of the monitoring period the average step varies
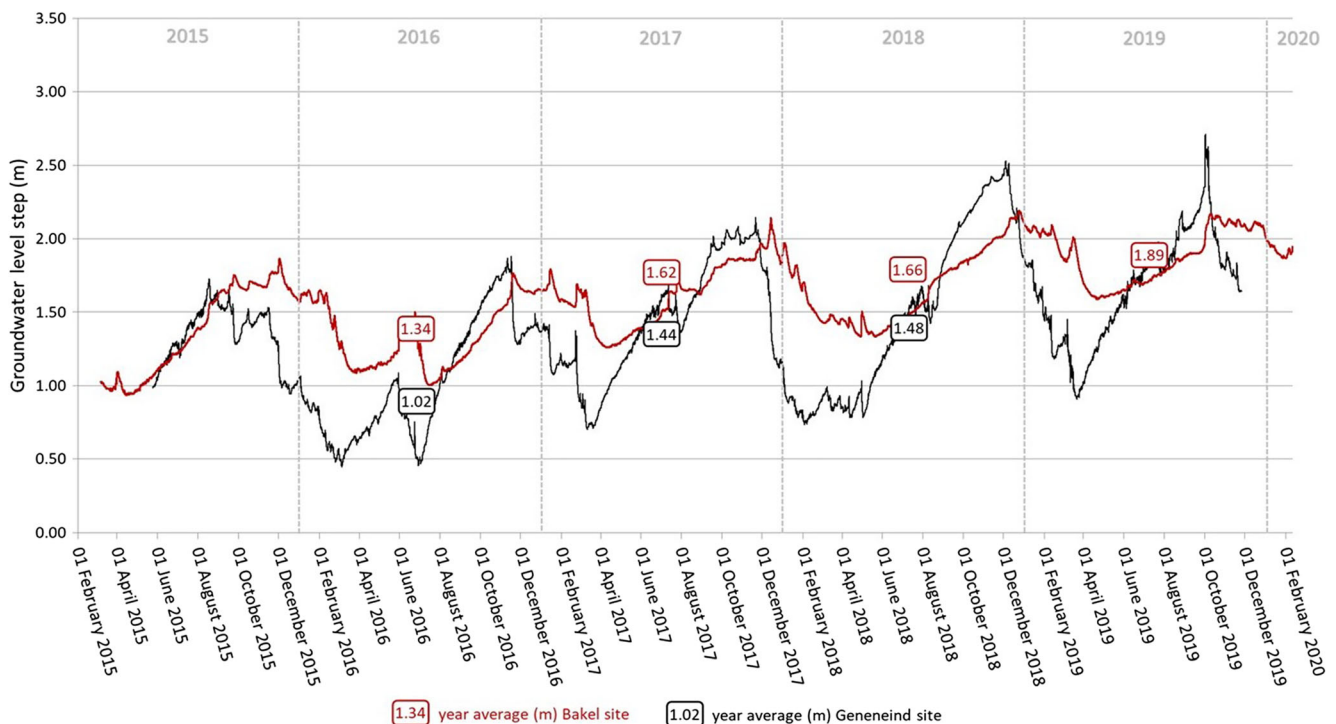


**Fig. 10** Temporal variation of the yearly average phreatic cross-fault groundwater-level step at the Bakel and Geneneind sites (2015–2020). At the Bakel site the average level step increases by 0.55 m, from 1.34 m (2016) to 1.89 m (2019), and at the Geneneind site the level step increases by 0.46 m, from 1.02 m (2016) to 1.48 m (2018)
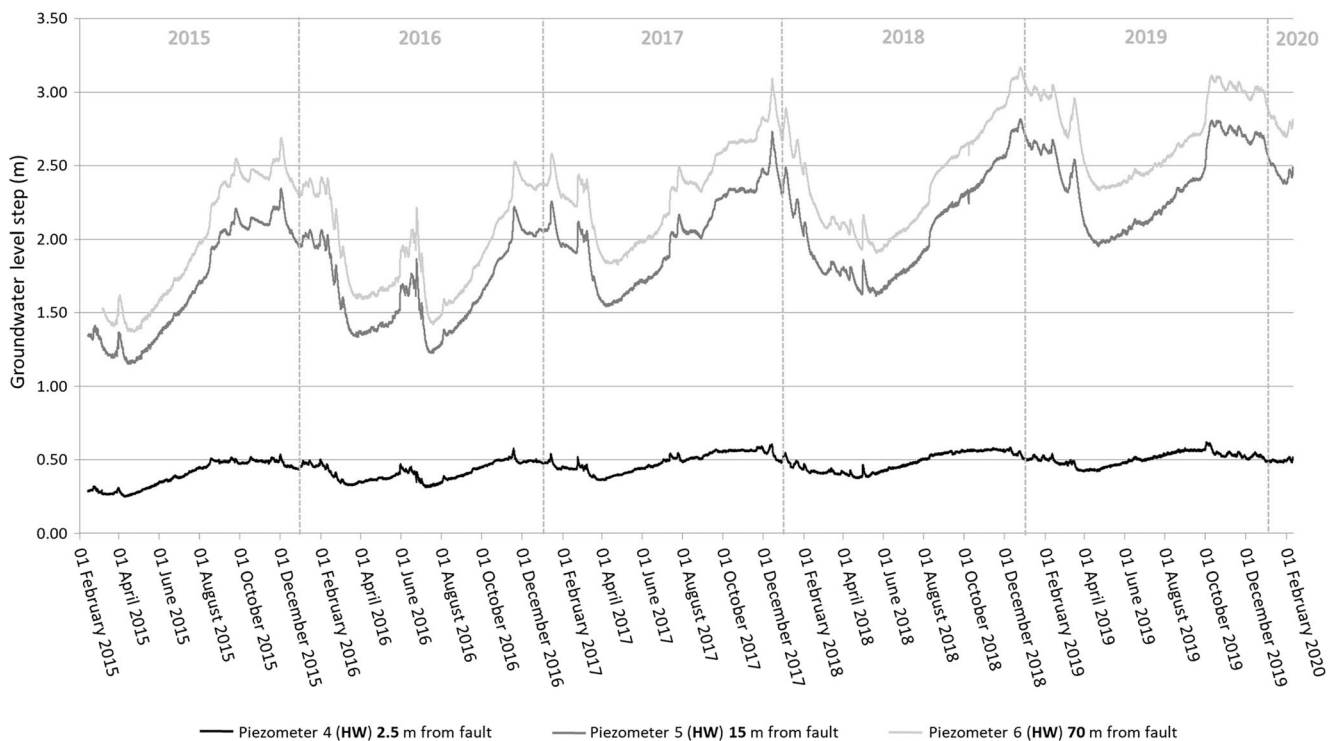
**Fig. 11** The phreatic cross-fault groundwater-level steps at the Bakel site (2015–2020), which increase with increasing distance to the fault of the measuring points on the hanging wall (HW). At 2.5 m from the fault (piezometer 4,) the average level step is smallest and ranges from 0.25 to 0.62 m, at 15 m from the fault (piezometer 5) the level step is larger and ranges from 1.15 to 1.85 m, and furthest away from the fault at 70 m (piezometer 6), the level step is largest and ranges from 1.37 to 3.17 m

between 1.05 and 2.09 m. A smaller (<1.05 m) or larger (>2.09 m) average step size only occurs 5% of the time.

The average annual groundwater-level step at the Bakel site is calculated by comparing the groundwater level on the foot wall (average from piezometers 1, 2, 3, 7 and 8) with the level on the hanging wall (average piezometers 4-6). The calculated step increased annually from 1.34 m in 2016, via 1.62 m in 2017 and 1.66 m in 2018, to 1.89 m in 2019 (Fig. 10). The Geneneind site indicates a similar trend with an increasing step from 1.02 m in 2016, via 1.44 m in 2017 to 1.48 m in 2018 (Fig. 10). Further, the phreatic cross-fault groundwater-level steps for both sites show a repetitive pattern with a maximum step around November–December–January, followed by a steep decline with a minimum average step in March–April–May (Fig. 10).

In addition to the variation and trend of the average phreatic cross-fault groundwater-level step, in which all piezometer results from the foot wall are compared with those from the hanging wall, the available time series also allow for calculating groundwater level steps with distance to the fault. At the Bakel site, the largest step is found when the groundwater levels in piezometer 3 are compared with those in piezometer 6 at approximately 70 m from the fault. The step size then varies from 1.37 to 3.17 m (Fig. 11). A similar comparison

between piezometer 3 and piezometer 5 at a distance of 15 m from the fault results in a smaller phreatic cross-fault groundwater-level step, ranging from 1.15 to 2.81 m (Fig. 11). A comparison between piezometer 3 on the foot wall and piezometer 4 on the hanging wall at respectively 2 and 2.5 m from the fault results in the smallest phreatic cross-fault phreatic groundwater-level step ranging from 0.25 to 0.62 m (Fig. 11).

The groundwater-level step directly across the approximately 1-m-wide fault zone at the Bakel site (Van Balen et al. 2019) was not measured, but it can be calculated by extrapolation. Using the average groundwater level of piezometers 4, 5 and 6 on the hanging wall, the groundwater level located directly at the hanging wall side of the fault was calculated at 20.72 m NAP. Similarly, a level of 20.89 m NAP directly at the fault on the foot wall side was determined using piezometers 1-3. The difference between both extrapolated levels (Fig. 12) shows that the average phreatic cross-fault groundwater-level step is 0.17 m. When using only piezometers 5 and 6 for extrapolation on the hanging wall, an average cross-fault level step of 1.91 m results (Fig. 12). See discussion for the implications of a small cross-fault level step for fault permeability and for the design of the near-fault monitoring networks.
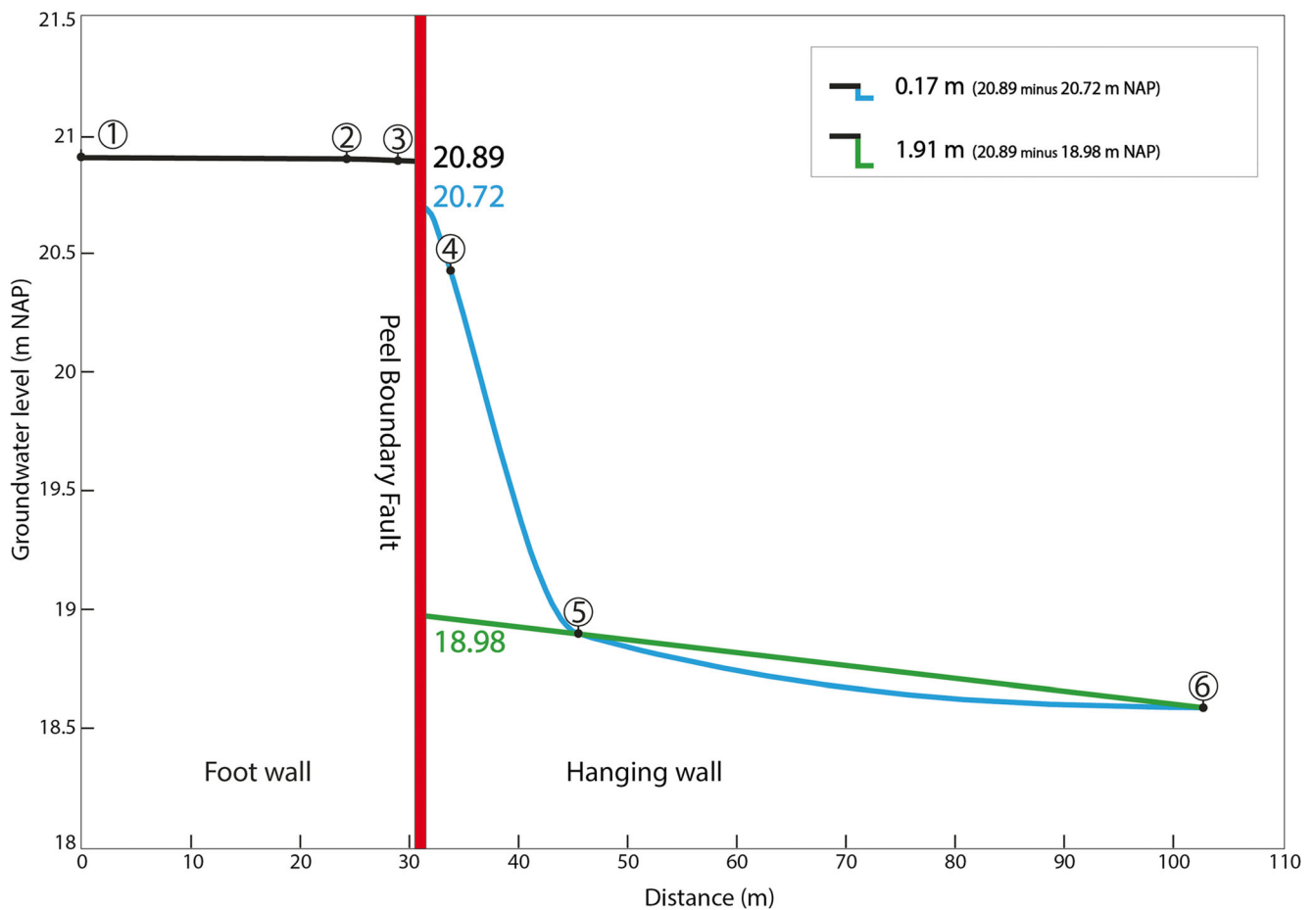
**Fig. 12** Extrapolation of phreatic groundwater levels from piezometers 1-3 on the foot wall towards the Peel Boundary Fault (PBF), which results in a level of 20.89 m NAP and is (almost) independent of the position of the piezometers. On the hanging wall, the groundwater levels do depend on the piezometer distance to the PBF, which is best illustrated by the effect of near-fault piezometer 4. Extrapolating groundwater levels from piezometer 6 via piezometer 5 towards the PBF results in a level of 18.98 m NAP and a corresponding cross-fault groundwater-level step of 1.91 m. When the groundwater levels from piezometer 4 are added to the extrapolation a level of 20.72 m is calculated and the groundwater-level step directly across the fault is 0.17 m

**Table 4** The average fit percentage (calculated as explained variance percentage: EVP) using precipitation and evapotranspiration as explaining variables of groundwater-level variation for all piezometers (time series) during the 2015–2020 period

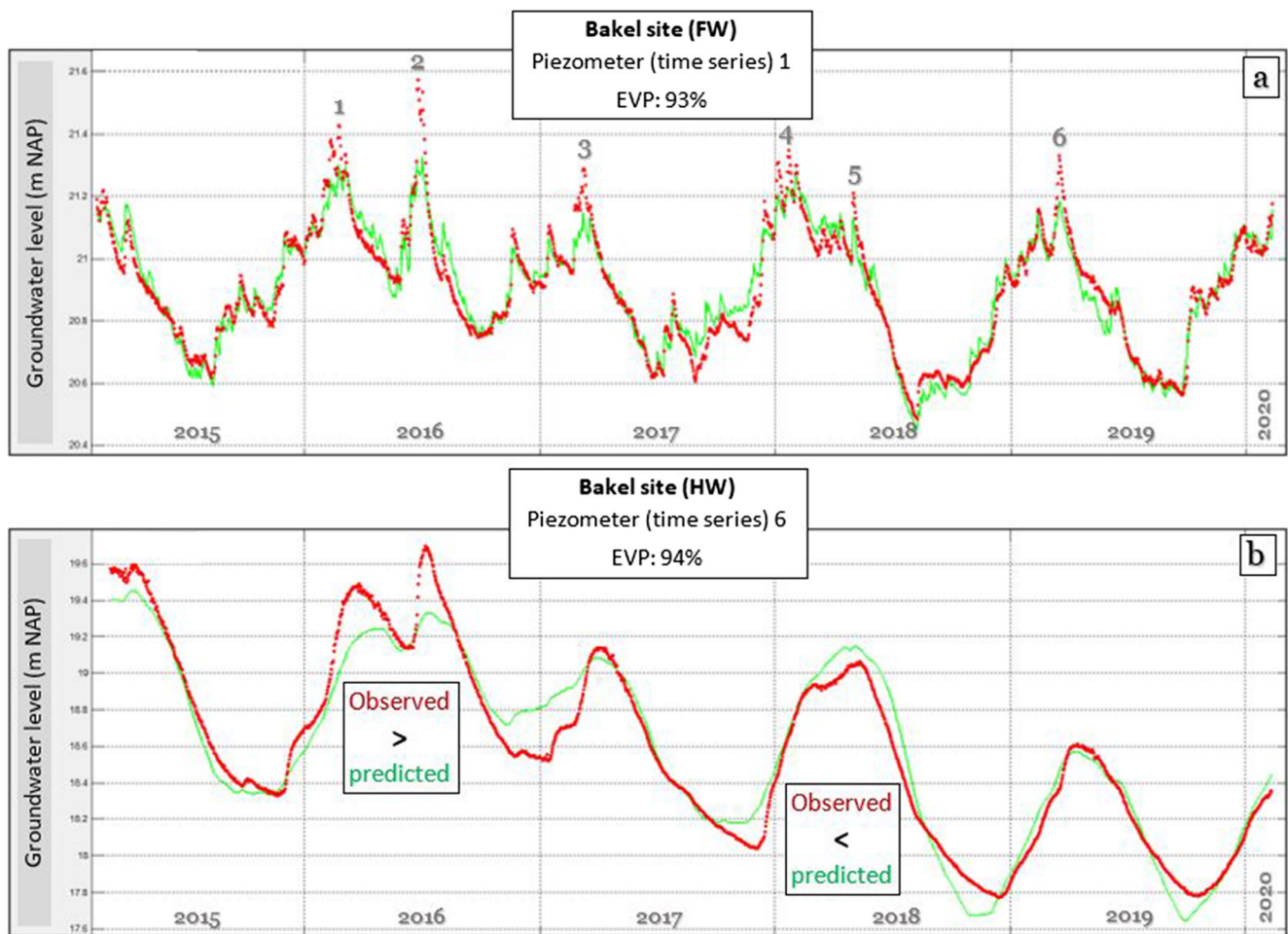| Bakel site | | Geneneind site | |
|---|---|---|---|
| Piezometer(time series) | Fit percentage (average) | Piezometer (time series) | Fit percentage (average) |
| Foot wall | | | |
| 1 (Fig. 13a) | 93% | A | 57% |
| 2 | 93% | B | 63% |
| 3 | 93% | C | 47% |
| 7 | 92% | D | 74% |
| 8 | 93% | E | 72% |
| – | 93% (average) | F | 68% |
| – | – | – | 64% (average) |
| Hanging wall | | | |
| 4 | 94% | G | 88% |
| 5 | 94% | H | 89% |
| 6 (Fig. 13b) | 94% | – | 89% (average) |
| – | 94% (average) | – | – |

**Fig. 13** **a** Explained variance percentage (EVP) for piezometer (time series) 1 on the foot wall (FW) at the Bakel site (2015–2020), with six short intervals (peaks) where the observed groundwater levels (red line) deviate from the predicted levels (green line) and **b** EVPs for piezometer (time series) 6 on the hanging wall (HW) showing longer lasting deviations

## Precipitation, evapotranspiration and groundwater-level variation

The influence of precipitation and evapotranspiration on groundwater-level variation for both sites during the 2015–2020 period is determined using statistical time-series analysis. The average fit percentage for each piezometer (time series) at the sites is shown in Table 4. For the Bakel site, the outcome of these calculations show an average fit between the predicted and the measured groundwater levels, calculated as explained variance percentage (EVP), of 92–94% for both the foot wall and hanging wall. At the Geneneind site, an almost similar average fit of 88–89% was calculated for groundwater-level variation on the hanging wall. A lower average fit was calculated for the time series on the foot wall of the Geneneind site (Table 4) varying from 47 to 74% (foot wall average 64%). An EVP below 70% (piezometers A, B, C and F) suggests insufficient data or additional factors such as the possible presence of land drainage or groundwater abstractions

influencing groundwater-level variation because these piezometers are located closer to agricultural land.

The fit percentage for the Bakel site, using precipitation and evapotranspiration as explaining variables, is on average very accurate (EVP > > 70%). However, the observed groundwater levels reveal intervals with deviations from the predicted levels (Fig. 13). Piezometer (time series) 1 on the foot wall (Fig. 13a) shows six short intervals (peaks) where the observed groundwater levels are occasionally 0.1–0.3 m higher than predicted. These peaks lasted between 7 days (peak 5) and 32 days (peak 4) and also occur in other foot-wall time series at both sites. The second peak in June–July 2016 (Fig. 13a) lasted 14 days and the recorded levels were underestimated with 0.3 m. During this time period 77 mm precipitation was recorded. All other deviations of peak groundwater levels are also characterized by above-average precipitation such as during peak 4 (32 days) when 110 mm of precipitation was recorded. Piezometer (time series) 6 on the hanging wall (Fig. 13b) reveals a pattern in which the

observed groundwater levels are higher and lower than predicted. These deviations extend over a longer period of time compared to the short outliers seen on the foot wall.

## Discussion

### Reduced fault-zone hydraulic conductivity

Nonfault horizontal hydraulic conductivity values from deposits around the Bakel site, obtained from the national database REGIS II v2.2 (Hummelman et al. 2019), range from 2.5 to 5.0 m day$^{-1}$ for fine-grained aeolian deposits to around 50–100 m day$^{-1}$ for the coarser Meuse River deposits. The observed average (near) fault horizontal hydraulic conductivity value at the Bakel site (Table 3) is 0.53 m day$^{-1}$ and is thus 1–3 orders of magnitude lower than those reported for similar lithologies away from the fault. The reduction in hydraulic conductivity can be explained by displacement and by past seismic activity of the fault. Fault displacement resulted in juxtaposition (Fig. 5d) of sedimentary deposits with strongly contrasting permeability (Fig. 5b) and is expected to have caused grain-scale mixing of silt and sand and the reorientation of elongated grains (Bense et al. 2003b). In general, seismic energy release during earthquakes results in shaking of the unconsolidated sediments causing liquefaction (Obermeier 1996). In turn, this likely results in porosity decrease, and thus lower permeability of the affected sediments. In the Bakel trench, this proposed explanation for permeability reduction is supported by liquefaction features such as the subvertical clastic dyke injected in the fault core (Fig. 5c), two smaller clastic dykes and flame structures (Van Balen et al. 2019). Apart from being evidence for seismicity-related effects such as compaction, the presence of a clastic dyke also resulted in a reduced horizontal hydraulic conductivity of 0.02 m day$^{-1}$ (Table 3; Fig. 5b). In addition to these physical mechanisms, permeability in the Bakel trench can also have been reduced geochemically through the precipitation of iron (hydro)oxides as shown by orange-coloured bands starting at the fault core and continuing on the hanging wall (Fig. 3).

The fault at the Bakel site acts as a barrier to groundwater flow causing a cross-fault groundwater-level step. Although the near-fault hydraulic conductivity values are substantially reduced (range: 0.003–4.43 m day$^{-1}$) compared to values from similar lithologies away from the fault (range: 2.5–100 m day$^{-1}$), they do not support the concept of the fault being an (almost) impermeable vertical barrier to horizontal groundwater flow as suggested by, e.g., Van den Boom et al. (2007) and Blom et al. (2009). The near-fault hydraulic conductivity values (Table 3) indicate a connection between the groundwater system in the foot wall and the system in the hanging wall as further demonstrated below (see section 'Fault-related

groundwater systems'). Thus, the fault in the Bakel site can best be characterized as semi-impermeable such as suggested in the literature elsewhere for poorly consolidated sedimentary aquifers (Bense et al. 2013).

### Fault-related groundwater systems

Near-surface groundwater levels *on the foot wall* and shallow levels directly across the fault on the hanging wall, show little spatial variability and display a spiky temporal variation pattern (Figs. 6, 7 and 8a). The characteristics of the phreatic groundwater system on the foot wall are explained by the fault-related hydrogeological setting. Being a semi-impermeable barrier, the fault hampers phreatic cross-fault groundwater flow and, as a consequence, the groundwater level rises on the foot wall during precipitation events. Because the regional topography-driven groundwater flow is obliquely directed towards the fault, the presence of the low-permeability fault also leads to upward groundwater flow (Reiner and Crocker 1990; López and Smith 1995; Bense and Kooi 2004; Lapperre et al. 2019) further contributing to high groundwater levels, and locally even seepage, on the foot wall close to the fault. At the Bakel and Geneneind sites, permanent high groundwater levels on the foot wall result in a shallow unsaturated zone causing a rapid response to (heavy) precipitation (Yan et al. 2018; Wittenberg et al. 2019) and to evapotranspiration (Soylu et al. 2011; Condon and Maxwell 2019) and explains the observed spiky temporal variation pattern.

Groundwater levels on the hanging wall and foot wall at both sites show distinct differences. *On the hanging wall*, groundwater levels are at much larger depth (Figs. 7, 8, and 14a), demonstrate a greater level variability, and have a smoother pattern (Figs. 7, 8, and 14a). This is explained by the effect of a groundwater system with a lower base level maintained by limited influx from groundwater from the foot wall, due to the presence of a semi-impermeable barrier separating the foot wall from the hanging wall, and by a hydrological system expected to have more output, e.g. via connected groundwater systems or surface water. In any case, due to these and related hydrogeological circumstances a deeper water table is measured which has knock-on effects on the dynamics of groundwater recharge and potential for evapotranspiration (e.g., delay in groundwater-level peaks and troughs relative to the foot-wall water-level time series), particularly for groundwater levels in piezometers 5 and 6. The shallower groundwater levels on the foot wall seem connected to the deeper levels in the hanging wall via a steep groundwater gradient across the fault (Figs. 7, 11 and 12). The combined effect of a fault with a barrier effect, water connectivity to the hanging wall groundwater system relative to the foot wall, and the declining topography of the hanging wall with lower groundwater levels (Fig. 14a) leads to an increase in thickness
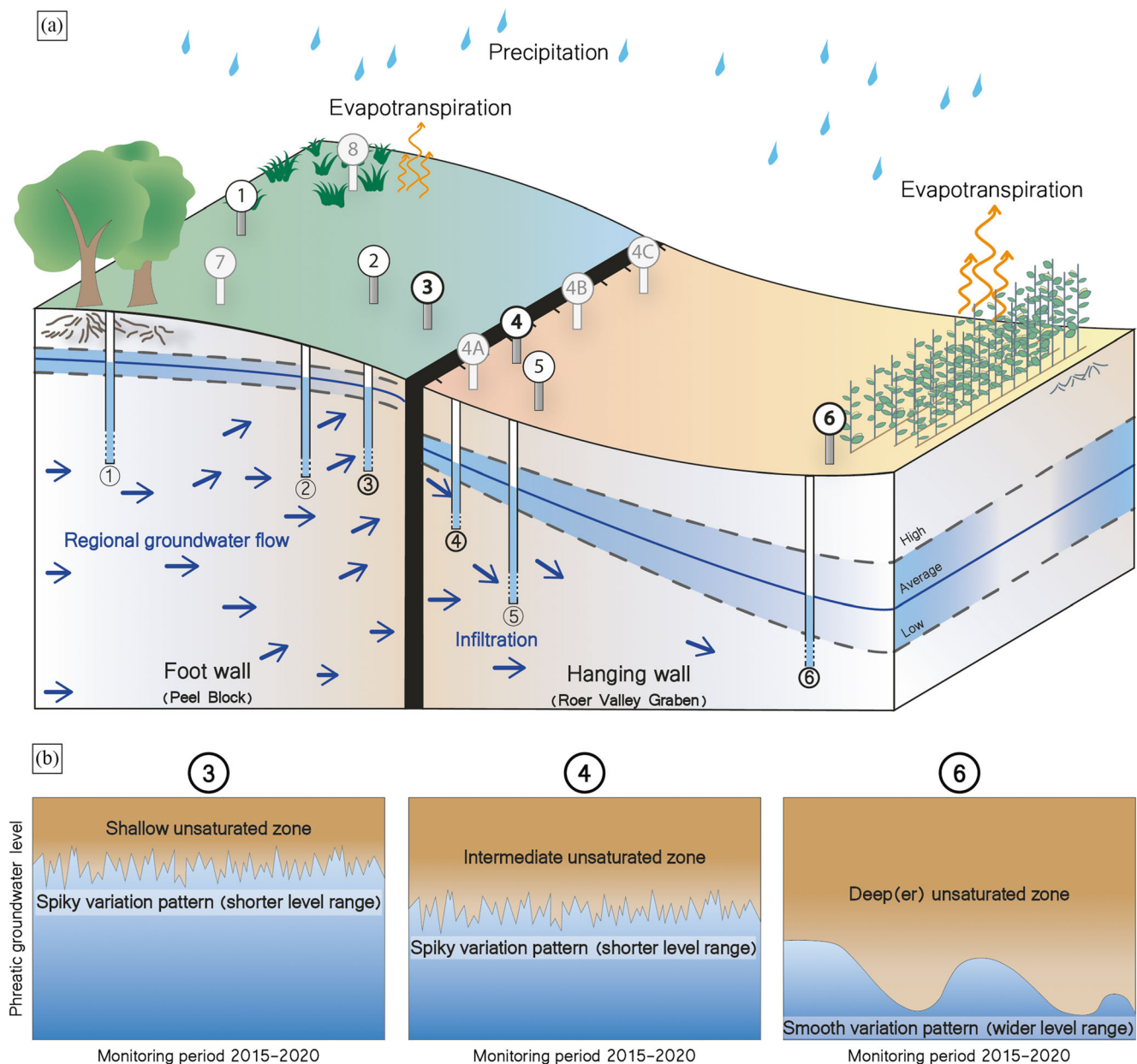
**Fig. 14 a** Block diagram of the Bakel site with a schematic impression of the groundwater system on the foot wall and hanging wall, the cross-fault groundwater-level step and location of the piezometers and **b** schematic impression of the spatial groundwater-level variation on the foot wall (piezometer 3), on the hanging wall (piezometers 4 and 6) and variable thickness of the unsaturated zone

of the unsaturated zone with increasing distance to the fault (Fig. 14b). The increasing thickness delays and reduces the effect of recharge and evapotranspiration on groundwater-level variations and is substantiated by the observed delay of peaks and troughs on the hanging wall compared to those on the foot wall (Fig. 7). It could be argued that, compared to the shallow groundwater system on the foot wall, the effect of evapotranspiration on groundwater-level variation on the hanging wall is much smaller, since capillary rise in sand is limited; the capillary fringe often does not reach the root zone and water availability for both evaporation and transpiration is therefore (frequently) restricted (Teuling et al. 2006; Zhang

and Schilling 2006). However, the effects of evapotranspiration on hanging-wall groundwater levels cannot be interpreted in isolation, but must be considered in conjunction with the presented characteristics of the corresponding groundwater system. Because of the expected limited effect of evapotranspiration and the absence of land drainage and groundwater abstractions in the vicinity of the Bakel site, precipitation variation appears to be the main parameter influencing (near) fault groundwater-level fluctuations on the hanging wall.

The measurement results from piezometer 4 (and 4A, 4B and 4C) on the hanging wall close to the fault (Fig. 5a) demonstrate a cross-fault groundwater-level step (Fig. 14a) but at

**Fig. 15** Digital elevation model based on AHN3 (2019) and block diagram showing in-between-fault water conservation and restoration of fault-related wet areas. Coordinate system is the Dutch 87 National Grid (RD) and levels with respect to the Dutch Ordnance Datum (NAP). **a** Plan view of a section of the Roer Valley Graben (RVG), Peel Boundary Fault zone (PBFZ) and Peel Block (PB) with (from west to east) the Peel Boundary Fault (PBF), Milheeze Fault (MF) and Griendtsveen Fault (GF) and **b** block diagram (cross section) showing the phreatic water table before conservation, impression of the regional flow direction (blue arrows), indication of the search area for in-between-fault water conservation and possible effect of a groundwater-level rise after conservation on nature restoration of fault-related wet areas with often iron-rich seepage (locally called *wijstgronden*)
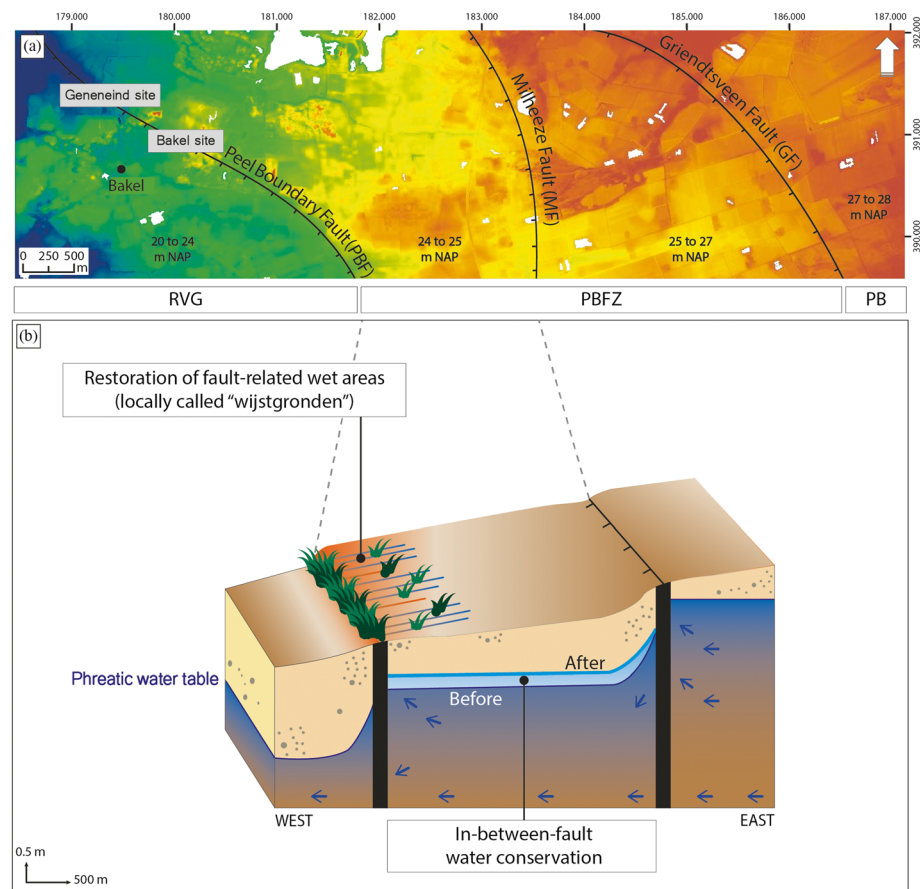


the same time show a spiky temporal variation pattern very similar to the observed pattern on the foot wall (Figs. 7 and 14b). These characteristics are attributed to the combined effect of the nearby semi-impermeable fault causing a cross-fault groundwater-level step and the relatively high groundwater levels just across the fault on the hanging wall (Figs. 7 and 12). This also seems to apply to piezometers G/H on the hanging wall of the Geneneind site (Fig. 4e). Although further away from the fault on the hanging wall than piezometer 4 at the Bakel site (and 4A–4C), piezometers G/H demonstrate a spiky variation pattern (Fig. 8a). In this case, the spikyness is probably caused by the local topography where a lower surface level results in a relatively high groundwater level. Level measurements from piezometers 4A–4C (Fig. 14a) further demonstrate that piezometer 4, closest to the fault on the hanging wall, is not affected by restoration of the fault at the Bakel site since they show similar levels and are located either outside the trench contour or have their filters below the trench floor in nonaffected (not restored) sediments.

The concept of a regional hydrological system with semi-impermeable barriers provides new opportunities for fault-related water conservation and nature restoration. Since the PBFZ consists of multiple northwest–southeast-oriented faults such as the PBF (Fig. 15a), a repetitive pattern of

groundwater systems with shallower and deeper groundwater levels is present. In particular, the in-between-fault systems and the presence of multiple faults with reduced permeability work to repeatedly slow down the horizontal groundwater flow could be suitable for temporary water conservation and contribute to the replenishment of the deeper groundwater system. This conservation causes the phreatic groundwater level to rise over time (Fig. 15b) and has a positive effect on restoration of groundwater-dependent ecosystems (Hoogland et al. 2010) such as the unique fault-related wet areas on the foot wall side of faults, locally called *wijstgronden* (Fig. 15b), which may be expected in the long term.

## Cross-fault groundwater-level step

The measurements demonstrate that cross-fault groundwater-level steps show temporal variation and spatial variability. The review by Lapperre et al. (2019) of fault-zone permeabilities and groundwater-level steps in the Roer Valley Rift System described the influence of distance between the measurement locations (piezometers) on the magnitude of the cross-fault groundwater-level step. A larger cross-fault groundwater-level step was found with increasing distance between, often sparsely available, piezometers. The monitoring array at

Bakel allows for a more detailed analysis of this distance to step-size correlation. The smallest average level step across the approximately 1-m-wide fault (Van Balen et al. 2019) was calculated by extrapolation to be 0.17 m (Fig. 12). A somewhat larger average groundwater level step of 0.46 m (Fig. 11) is found without extrapolation, if only piezometer 4, at 2.5 m from the fault, is used to characterize the magnitude of the water-table step across the fault. At 15–70 m from the fault, the extrapolated average cross-fault groundwater-level step increases to 1.91 m (Fig. 12). Determining the minimum cross-fault groundwater-level step is an important element to improve groundwater modelling of faults on a detailed scale and to optimize field monitoring to collect useful data.

## Implications for groundwater modelling

For detailed numerical modelling of fault-zone hydrogeology, e.g., to calculate the opportunities for in-between-fault water conservation and study the effect on restoration of fault-related wet areas, hydraulic conductivity values can best be measured in situ (Table 3) or inferred from the minimum cross-fault groundwater-level step (Fig. 12). When using inferred hydraulic conductivity values from *regional* groundwater models (Fig. 2d), often based on large cross-fault groundwater-level steps derived from measurements in piezometers at a larger separation distance, it is likely that (near) fault permeability is underestimated. Fault modelling at a smaller observational scale can also be applied to elaborate on previously performed calculations to quantify groundwater flow in and around fault zones (Haneberg 1995; Bense 2002) and develop new concepts for field monitoring particularly accounting for the steep groundwater level decline present on the hanging wall near the fault (Fig. 12).

## Weather data and climatic trends

The precipitation and evapotranspiration data from nearby weather station Eindhoven, west of the Bakel and Geneneind sites, was used to perform the Menyanthes analyses. The highest EVP for the 2015–2020 time series of the Bakel site is 92–94% (Table 4). This demonstrates that precipitation and evapotranspiration almost fully account for the observed level variation, and additional explanatory variables such as the presence of land drainage, groundwater abstraction and variable surface-water levels, are of minor importance. The EVP values of the Geneneind site for the 2015–2020 groundwater-level time series on the hanging wall (Table 4) are also high (88–89%), again showing precipitation and evapotranspiration as the main explanatory variables. Although there is a very high EVP for these time series, the statistical analysis systematically underestimates peak levels on the foot wall (Fig. 13a) caused by above-average precipitation events. These short peaks are due to the shallow

unsaturated zone (Fig. 14b) and corresponding short response time of the phreatic groundwater level. On the hanging wall, the statistical time-series analysis underestimates or overestimates groundwater levels. The greater difference in magnitude between predicted and observed levels on the hanging wall (Fig. 13b), as well as the differences in timing of some peaks and troughs in water levels, is likely to result from a deeper unsaturated zone in the hanging wall, particularly at piezometer 6 (Fig. 14b). The time series from the foot wall at the Geneneind site shows a lower EVP (Table 4) likely due to intervals lacking level recording related to occasional malfunctioning of data loggers.

Future climate scenarios for the Netherlands (KNMI 2015) predict an average temperature rise (1–2 °C), more precipitation (2.5–5.5%) including downpours, and an increase in evapotranspiration (3–7%) by 2050. These changes may affect groundwater level variation, cross-fault groundwater levels and opportunities for fault-related water conservation. The spiky temporal variation pattern on the foot wall may be intensified by the predicted effect of prolonged droughts followed by downpours in combination with a shallow unsaturated zone (Fig. 14b). A groundwater level rise on the foot wall is uncertain, because the predicted temperature rise may increase evapotranspiration rates and therefore (partially) mitigate the effect of more precipitation. Groundwater levels on the hanging wall are expected to respond more slowly and more gradually to the predicted climatic changes because of a deep(er) unsaturated zone (Fig. 14b). Additionally, a tendency towards higher groundwater levels on the hanging wall is expected due to an increase in annual precipitation and an expected limited effect of higher evapotranspiration. If the climatic effects indeed differ for the groundwater system on the foot wall and on the hanging wall, a more variable future cross-fault groundwater-level step is expected. A decrease in precipitation also seems to have an important effect. The average cross-fault groundwater-level step at the Bakel site (available: 2016–2019) increased during the monitoring period by 0.55 m and at the Geneneind site (available: 2016–2018) by 0.46 m (Fig. 10). The increasing step at both sites is explained by the cumulative effect of the above-average dry years 2017 (720 mm), 2018 (630 mm) and 2019 (708 mm). Less precipitation than the 30-year (1991–2020) average of 749 mm (KNMI, 2022) during these three consecutive years has resulted in a lowering of the water table (Figs. 7 and 8) of the precipitation-dependent groundwater system in the hanging wall. These dry years seem to have had little impact on the foot-wall groundwater system (Figs. 6 and 8), where consistently high levels with relatively little variation were recorded as a result of a constant topography-driven regional groundwater flow (Fig. 14a) and a shallow unsaturated zone (Fig. 14b). Finally, it should be noted that the interpretation of the results of this detailed hydrogeological study on cross-fault level differences, the reconstruction of the cross-fault

groundwater-level step, and the inferences about the influence of precipitation and evapotranspiration is inconclusive about possible effects from regional topography, deep groundwater abstractions and surface-water bodies at a distance from the Bakel and Geneneind sites.

## Conclusions

The results of the Bakel and Geneneind site studies at the Peel Boundary Fault in the Roer Valley Rift System indicate that the fault is semi-impermeable to groundwater flow, and not impermeable as generally assumed. This is evidenced by the following findings:

- The hydraulic conductivity measurements show reduced permeability values. However, these values do not indicate the fault being fully impermeable to groundwater flow. Fault hydraulic conductivity values at the Bakel site range from 0.003 to 4.43 m day$^{-1}$, whereas conductivity values from similar sediments away from the fault are in the range of 2.5–100 m day$^{-1}$.
- There is a cross-fault groundwater-level step and a water table sloping away from the fault on the hanging wall. The sloping water table in the hanging wall is most likely explained by a lateral influx of groundwater from the foot wall through the approximately 1-m-wide fault zone. Extrapolation of groundwater levels to the fault zone (on the hanging wall and on the foot wall) shows that the groundwater level step across the fault is in the order of 0.2 m. The small cross-fault-step size is consistent with the results of the conductivity measurements.
- There is a characteristic difference between the groundwater system in the foot wall and in the hanging wall. In the foot wall, the water table is high (near surface), subhorizontal and rapidly responds to precipitation events. In the hanging wall, the water table slopes away from the fault, and the response to precipitation events is delayed due to a buffering effect of the unsaturated zone. Based on the fact that the groundwater-level-variation pattern in piezometer 4 at the Bakel site, located at only 2.5 m away from the fault on the hanging wall, is lower and largely resembles level variations on the foot wall, it is inferred that groundwater flows through a semi-impermeable fault zone.
- Precipitation of iron (hydro)oxides occurs on the hanging wall. Within the excavation depth of the Bakel trench, orange-coloured iron precipitation bands were observed starting from the fault and expanding into the hanging wall. The precipitation pattern suggests the supply of iron-rich groundwater from the foot wall through the fault zone into the hanging wall, with a maximum precipitation effect in the coarser sand and gravelly sand deposits bordering the fault.

The 0.2-m-cross-fault-step size is significantly less than the commonly inferred 1–2-m-step height which is based on piezometers at tens to hundreds of metres distance from the fault. These erroneous groundwater step heights cause regional groundwater models to assume too low values for fault hydraulic conductivity. The groundwater level steps do however also show temporal variations, which are largely explained by variation in precipitation and evapotranspiration. In addition to the commonly accepted mechanisms for reduction of permeability in fault zones, like clay smearing, grain-reorientation and juxtaposition, the reduced permeability at the Bakel site is additionally explained by fluidizations, resulting in an expected loss of porosity and thus permeability.

## Declarations

**Conflict of interest** On behalf of all authors, the corresponding author states that there is no conflict of interest.

## References

AHN3 (2019) Actueel Hoogtebestand Nederland [Current Dutch elevation]. https://www.ahn.nl/. Accessed 1 March 2021

Balsamo F, Storti F (2010) Grain size and permeability evolution of soft-sediment extensional sub-seismic and seismic fault zones in high-

porosity sediments from the Crotone basin, southern Apennines, Italy. Mar Pet Geol 27(4):822–837. https://doi.org/10.1016/j.marpetgeo.2009.10.016

Bense VF (2002) Hydrogeologische karakterisering van breukzones in Zuidoost-Nederland [Hydrogeological characterization of fault zones in southeast Netherlands]. Stromingen 8(3):17–30

Bense VF (2004) The hydraulic properties of faults in unconsolidated sediments and their impact on groundwater flow: a study in the Roer Valley Rift System and adjacent areas in the Lower Rhine Embayment. PhD Thesis, VU University Amsterdam, The Netherlands

Bense VF, Kooi H (2004) Temporal and spatial variations of shallow subsurface temperature as a record of lateral variations in groundwater flow. J Geophys Res Solid Earth 109(B4). https://doi.org/10.1029/2003JB002782

Bense VF, Van Balen RT (2004) The effect of fault relay and clay smearing on groundwater flow patterns in the Lower Rhine Embayment. Basin Res 16(3):397–411. https://doi.org/10.1111/j.1365-2117.2004.00238.x

Bense VF, Van Balen RT, De Vries JJ (2003a) The impact of faults on the hydrogeological conditions in the Roer Valley Rift System: an overview. Neth J Geosci 82(1):41–54. https://doi.org/10.1017/S0016774600022782

Bense VF, Van den Berg EH, Van Balen RT (2003b) Deformation mechanisms and hydraulic properties of fault zones in unconsolidated sediments; the Roer Valley Rift System, The Netherlands. Hydrogeol J 11:319–332. https://doi.org/10.1007/s10040-003-0262-8

Bense VF, Gleeson T, Loveless SE, Bour O, Scibek J (2013) Fault zone hydrogeology. Earth Sci Rev 127:171–192. https://doi.org/10.1016/j.earscirev.2013.09.008

Bense VF, Shipton ZK, Kremer Y, Kampman N (2016) Fault zone hydrogeology: introduction to the special issue. Geofluids 16(4):655–657. https://doi.org/10.1111/gfl.12205

Blom M, Paulissen MPCP, Geertsema W, Agricola HJ (2009) Klimaatverandering in drie casestudiegebieden: integratie van adaptatiestrategieën voor landbouw en natuur [Climate change in three case-study areas: integration of adaptation strategies for agriculture and nature]. Plant Research International Report 255, Wageningen University and Research, Wageningen, The Netherlands

Bokanda EE, Ekomane E, Eyong JT, Njilah IK, Ashukem EN, Bisong RN, Bisse SB (2018) Genesis of clastic dykes and soft-sediment deformation structures in the Mamfe Basin, south-west region, Cameroon: field geology approach. J Geol Res 2018(3749725). https://doi.org/10.1155/2018/3749725

Condon LE, Maxwell RM (2019) Simulating the sensitivity of evapotranspiration and streamflow to large-scale groundwater depletion. Sci Adv 5(6). https://doi.org/10.1126/sciadv.aav4574

Deckers J, Van Noten K, Schiltz M, Lecocq T, Vanneste K (2018) Integrated study on the topographic and shallow subsurface expression of the Grote Brogel Fault at the boundary of the Roer Valley Graben, Belgium. Tectonophysics 722:486–506. https://doi.org/10.1016/j.tecto.2017.11.019

Eijkelkamp (2017) Laboratory permeameters user manual: version 2017–03. Eijkelkamp Soil and Water, Giesbeek, The Netherlands

Elbers JA, Moors EJ, Jacobs CMJ (2009) Gemeten actuele verdamping voor twaalf locaties in Nederland [Measured actual evaporation for twelve locations in the Netherlands]. Alterra report 1920, Alterra Wageningen University and Research, Wageningen, The Netherlands

Gunduz O, Simsek C (2011) Influence of climate change on shallow groundwater resources: the link between precipitation and groundwater levels in alluvial systems. Climate Change and its effects on water resources (NATO Science for Peace and Security Series C) 3: 225–233. https://doi.org/10.1007/978-94-007-1143-3_25

Haneberg WC (1995) Steady state groundwater flow across idealized faults. Water Resour Res 31(7):1815–1820. https://doi.org/10.1029/95WR01178

Higham DJ, Higham NJ (2017) MATLAB Guide, 3rd edition. Society for Industrial and Applied Mathematics, Philadelphia, PA

Hoogland T, Heuvelink GBM, Knotters M (2010) Mapping water-table depths over time to assess desiccation of groundwater-dependent ecosystems in the Netherlands. Wetlands 30:137–147. https://doi.org/10.1007/s13157-009-0011-4

Hummelman J, Maljers D, Menkovic A, Reindersma R, Stafleu J, Vernes R (2019) Totstandkomingsrapport hydrogeologisch model (REGIS II) [Final report hydrogeological model REGIS II]. TNO Report 2019 R11654, TNO, Utrecht, Belgium

Kasse C, Vandenberghe D, De Corte F, Van Den Haute P (2007) Late Weichselian fluvio-aeolian sands and coversands of the type locality Grubbenvorst (southern Netherlands): sedimentary environments, climate record and age. J Quat Sci 22:695–708. https://doi.org/10.1002/jqs.1087

KNMI (2000) Handbook for the meteorological observation. KNMI, De Bilt, The Netherlands

KNMI (2015) KNMI'14-klimaatscenario's voor Nederland [KNMI'14 climate scenarios for the Netherlands]. KNMI, De Bilt, The Netherlands

KNMI (2022) Online precipitation data from Koninklijk Nederlands Meteorologisch Instituut [Royal Netherlands Meteorological Institute KNMI]. https://cdn.knmi.nl/knmi/map/page/klimatologie/gegevens/maandgegevens/mndgeg_370_rh24.txt. Accessed December 2021

Lapperre RE, Smit HMC, Simmelink HJ, Van Lanen HAJ (1996) Variatie in permeabiliteit van een pleistocene rivierafzetting en de invloed op grondwaterstroming [Variation in permeability of a Pleistocene river deposit and its influence on groundwater flow]. $H_2O$ 29(18):520–523

Lapperre RE, Kasse C, Bense VF, Woolderink HAG, Van Balen RT (2019) An overview of fault zone permeabilities and groundwater level steps in the Roer Valley Rift System. Neth J Geosci 98. https://doi.org/10.1017/njg.2019.4

López DL, Smith L (1995) Fluid flow in fault zones: analysis of the interplay of convective circulation and topographically driven groundwater flow. Water Resour Res 31(6):1489–1503. https://doi.org/10.1029/95WR00422

Michon L, Van Balen RT (2005) Characterization and quantification of active faulting in the Roer Valley Rift System based on high precision digital elevation models. Quat Sci Rev 24(3–4):455–472. https://doi.org/10.1016/j.quascirev.2003.11.009

Michon L, Van Balen RT, Merle O, Pagnier H (2003) The Cenozoic evolution of the Roer Valley rift system integrated at a European scale. Tectonophysics 367:101–126. https://doi.org/10.1016/s0040-1951(03)00132-x

NEN-EN-ISO (2019) Geotechnical investigation and testing: laboratory testing of soil, part 11: permeability tests. ISO 17892-11:2019, International Organization for Standardization (ISO), Delft, The Netherlands

Obermeier SF (1996) Use of liquefaction-induced features for paleoseismic analysis: an overview of how seismic liquefaction features can be distinguished from other features and how their regional distribution and properties of source sediment can be used to infer the location and strength of Holocene paleo-earthquakes. Eng Geol 44(1–4):1–76. https://doi.org/10.1016/S0013-7952(96)00040-3

Reiner SR, Crocker MC (1990) Some effects of groundwater discharge through Mount Enterprise Fault Zone on surface water composition in southern Rusk County, Texas. https://www.searchanddiscovery.com/abstracts/html/1990/annual/abstracts/0748.htm. Accessed February 2022

Rhodes EJ (2011) Optically stimulated luminescence dating of sediments over the past 200,000 years. Annu Rev Earth Planet Sci 39:461–488. https://doi.org/10.1146/annurev-earth-040610-133425

Soylu ME, Istanbulluoglu E, Lenters JD, Wang T (2011) Quantifying the impact of groundwater depth on evapotranspiration in a semi-arid grassland region. Hydrol Earth Syst Sci 15(3):787–806. https://doi.org/10.5194/hess-15-787-2011

Taheri S, Ghomeshi S, Kantzas A (2017) Permeability calculations in unconsolidated homogeneous sands. Powder Technol 321:380–389. https://doi.org/10.1016/j.powtec.2017.08.014

Teuling AJ, Seneviratne SI, Williams C, Troch PA (2006) Observed timescales of evapotranspiration response to soil moisture. Geophys Res Lett:33(23). https://doi.org/10.1029/2006GL028178

Van Balen RT, Houtgast RF, Cloetingh SAPL (2005) Neotectonics of the Netherland: a review. Quat Sci Rev 24(3–4):439–454. https://doi.org/10.1016/j.quascirev.2004.01.011

Van Balen RT, Bakker MAJ, Kasse C, Wallinga J, Woolderink HAG (2019) A late glacial surface rupturing earthquake at the Peel boundary fault zone, Roer Valley Rift System, the Netherlands. Quat Sci Rev 218:254–266. https://doi.org/10.1016/j.quascirev.2019.06.033

Van den Boom B, Bossenbroek P, Holtland J (2007) 10 jaar hoogveenregeneratie in de Peel [10 years regeneration of a raised bog system]. De Levende Natuur 108(4):155–161

Vanneste K, Meghraouib M, Camelbeeck T (1999) Late Quaternary earthquake-related soft-sediment deformation along the Belgian portion of the Feldbiss fault, Lower Rhine Graben System. Tectonophysics 309(1–4):57–79. https://doi.org/10.1016/S0040-1951(99)00132-8

Von Asmuth JR (2012) Groundwater System Identification through time series analysis. PhD Thesis, Technische Universiteit Delft, The Netherlands

Wittenberg H, Aksoy H, Miegel K (2019) Fast response of groundwater to heavy rainfall. J Hydrol 571:837–842. https://doi.org/10.1016/j.jhydrol.2019.02.037

Yan S-F, Yu S-E, Wu Y-B, Pan D-F, Dong J-G (2018) Understanding groundwater table using a statistical model. Water Sci Eng 11(1):1–7. https://doi.org/10.1016/j.wse.2018.03.003

Zaadnoordijk WJ, Bus SAR, Lourens A, Berendrecht WL (2018) Automated time series modeling for piezometers in the National Database of The Netherlands. Groundwater 57(6):834–843. https://doi.org/10.1111/gwat.12819

Zhang Y-K, Schilling KE (2006) Effects of land cover on water table, soil moisture, evapotranspiration, and groundwater recharge: a field observation and analysis. J Hydrol 319(1–4):328–338. https://doi.org/10.1016/j.jhydrol.2005.06.044